SLAC – PUB – 4047
August 1986
(I)

DESIGN, CONSTRUCTION, PROTOTYPE TESTS AND PERFORMANCE OF A VERTEX CHAMBER FOR MAC*

W. W. Ash, H. R. Band, E. D. Bloom, M. Bosman† , T. Camporesi†,
G. B. Chadwick, M. C. Delfino, S. De Simone, W. T. Ford, M. W. Gettner,
G. P. Goderre‡ , D. E. Groom, R. B. Hurst, J. R. Johnson, K. H. Lau‡,
T. L. Lavine, R. E.Leedy, I. Lippi* , T. Maruyama, R. L. Messner,
J. H. Moromisato, L. J. Moss, F. Muller†, H. N. Nelson, I. Peruzzi,
M. Piccolo, R. Prepost, J. Pyrlik, N. Qi, A. L. Read, Jr.◇ ,
D. M. Ritson, L. J. Rosenberg, W. D. Shambroom♮ , J. C. Sleeman, J. G. Smith,
J. P. Venuti, P. G. Verdini, R. Weinstein, D. E. Wiser, and R. W. Zdarko

Department of Physics, University of Colorado, Boulder, Colorado 80309, and
I. N. F. N., Laboratori Nazionali di Frascati, Frascati, Italy, and
Department of Physics, University of Houston, Houston, Texas 77004, and
Department of Physics, Northeastern University, Boston, Massachusetts 02115, and
Department of Physics and Stanford Linear Accelerator Center,
Stanford University, Stanford, California 94305, and
Department of Physics, University of Utah, Salt Lake City, Utah 84112, and
Department of Physics, University of Wisconsin, Madison, Wisconsin 53706

Submitted to *Nuclear Instruments and Methods*

---

* This work was supported in part by the Department of Energy under contract numbers DE-AC02-81ER40025 (CU), DE-AC03-76SF00515 (SLAC), and DE-AC02-76ER00881 (UW); by the National Science Foundation under grant numbers NSF-PHY82-15133 (UH), NSF-PHY82-15413 and NSF-PHY82-15414 (NU), and NSF-PHY83-08135 (UU); and by the Istituto Nazionale di Fisica Nucleare.

† Permanent address: CERN, Geneva, Switzerland.
‡ Current address: Texas Accelerator Center, The Woodlands, TX 77380.
⋆ Current address: Physics Department, University of Padua, Padua, Italy.
◇ Now at University of Oslo, Oslo, Norway.
♮ Joint appointment Department of Physics and College of Computer Science, Northeastern University.

ABSTRACT

We describe the design considerations, contruction techniques, prototype tests and performance after installation, of a pressurized drift chamber constructed for use with the MAC detector at PEP. The chamber consists of 324 aluminized mylar tubes of 7 mm diameter with wall thickness of 100μm. With appropriate shielding it operates successfully at 3.6 cm from the beam line. It was simple to construct and is configured to permit any malfunctioning tubes to be remotely disconnected without affecting the overall operation.

We also describe resolution studies with a prototype chamber, in a SLAC test beam, over a wide range of gases and operating conditions. These proved that resolutions in the 10-50μm range were possible.

The chamber has operated without problems for two years in the PEP environment with a gas mixture of 50:49:1 of argon:CO_2:methane at 4 torr. The effective operating resolution averaged over all tubes is 50μm. The time to distance relation for this gas mixture, along with the geometric positioning of individual wires relative to the central tracking chamber, was obtained by calibrating with tracks from beam–beam interactions.

Our experience demonstrates that chambers of this type provide high precision tracking and are particularly suited for operation in regions with difficult physical access and/or high ambient radiation levels.

1. Introduction

The measurement of a comparatively long lifetime associated with particles containing b-quarks provided the motivation to upgrade the tracking capability of the PEP detector MAC with a Vertex Chamber (VC) of sufficient precision to measure particle flight paths of less than 1 mm. Prior to upgrading, the MAC detector relied on a Central Drift (CD) chamber with a position resolution of about 180–200μm and with the first layer of wires placed at a radius of 12 cm.

The objective of the upgrade was to add a high precision vertex chamber without modifying the existing tracking chamber. Since there was no space between the CD and the beam pipe, this mandated the construction of a device much closer to the circulating beams of an e^+e^- storage ring than had previously been attempted. Shielding studies led us to believe that this was feasible and indeed the observed radiation levels were close to expectations.

The detector had to be capable of operating in a region both difficult to get to and which was exposed to high ambient radiation levels. The time available for production of a fully operational chamber, including prototype and design studies was one year, ruling out the use of solid state or other new technologies. Since the best chamber lifetimes obtained to date are associated with flat cathodes, as opposed to wire configurations, and since a broken wire would be contained within a tube, we were led to consider a "straw chamber" (*i.e.* a chamber of small diameter coaxial wire tubes) adapted from the HRS collaboration design[1]. Further design considerations, described below, convinced us that this choice was best for us.

Monte Carlo and analytical studies[2] based on the programs and work of Vavra[3], Jaros[4], Boyarsky[5] and others, provide general guidelines for obtaining high resolution with drift chambers. Briefly they can be summarized as follows:

(a) The use of high gas pressures and short drift distances reduces the effect of diffusion on the drifting electrons. High gas pressures also improve track localization by increasing ionization density and consequently reduces fluctuation effects.

(b) The use of good electronic signal processing affords sensitivity to the first arriving electrons, which provides the best time determination, at least for short drift distances. This technique necessitates the use of relatively high gain operation of the chamber and, to prevent spurious pulses, requires relatively low cross-talk from neighboring channels.

(c) The use of a gas with relatively good diffusion characteristics is generally required. However, for short drift distances diffusion is not a

severe limitation, and in our tests a relatively wide range of gas mixtures provided adequate diffusion characteristics to meet our resolution goals.

Potential problems are associated with:

(a) The variable electric field leading to non–constant drift velocities.

(b) Mechanical alignment tolerance problems leading to possible electrostatic wire movements at high electrical gradients.

(c) Loss of resolution near the wire, which occurs in all chambers but which, in a small cell device, represents a possibly substantial part of the coverage.

As described below these problems were in large measure overcome and did not limit operation.

The advantages of the technique are:

(a) Chamber construction based on tubes is inherently simple. Each tube can be independently tested in place and the chamber can be designed so that any malfunctioning tube may be separately disconnected without affecting overall operation of the system.

(b) The tube configuration provides a large cathode area and minimizes cathode associated problems. It further functions as a cylindrical transmission line which is comparatively well shielded against cross-talk between neighboring elements, especially if it is terminated with its characteristic impedance.

(c) It is easily seen that the cylindrical geometry gives optimal collection for timing off the first arriving electron.

(d) Finally, the fact that drift cells are identical makes creating a calibration procedure easier.

In the following sections we describe our program of design, construction, testing and data handling for the chamber, emphasizing those aspects that we believe will be useful to others engaged in similar work. We first discuss the radiation shielding used, since it is an essential ingredient in the success of the chamber operation, then we give the final design of the chamber itself. Next we present construction details and describe the electronics and gas handling equipment. After these details are covered, we describe the results of tests which were performed with a prototype setup, and give data obtained for gas mixtures and conditions not used in the final experimental situation.

The final section of the paper describes the performance of the actual chamber during two years of operation and the software techniques used to auto–calibrate the time to distance conversion parameters and simultaneously obtain the small but essential corrections to the geometrical survey parameters. Pattern recognition techniques are briefly described, and finally we give the observed effective resolution.

2. Shielding Design

Owing to damage to the MAC beam pipe early in the operation of the detector, MAC was operated for a short period with minimal shielding and a temporary beam pipe of 2.1 mm thick 63 mm inner diameter stainless steel. We observed that under these conditions backgrounds were highly dependent on steering and on beam quality. When properly tuned, the increase in background hits in the central tracking chamber was surprisingly small and did not appreciably degrade pattern recognition. However the radiation levels did cause extra DC current to be drawn by the chamber and surges causing current trips through Malter breakdown, which would be unacceptable for long term operation.

We deduced that the main background for the chamber configuration planned would come from beam particles that had lost substantial energy by bremstrahlung in the long straight sections and were then over-focussed by the "low–beta" quadrupoles around the Interaction Region (IR), which could cause them to strike the vacuum pipe in the vicinity of the tracking chamber. We then estimated that, for long term stable operation with a small diameter beam pipe, additional shielding, sufficient to provide at least an order of magnitude reduction in backgrounds, would be required.

To achieve this reduction we imposed three conservative design criteria to ensure shielding from primary background sources. These criteria had to apply over the range of allowed tolerances for beam steering in the machine.

(a) The beam pipe in the neighbourhood of the vertex and central tracking chambers should be geometrically shadowed by collimators from overfocussed electrons. Additional shielding is also necessary between these collimators and the chambers to reduce the secondary radiation to safe levels.

(b) The beam pipe should also be shadowed from the synchrotron radiation produced by passage of the beam through the PEP magnets and from the low–beta quadrupoles close to the IR.

(c) Electrons, undergoing Coulomb scattering by the residual gas in the vacuum chamber ahead of the IR, should be intercepted by more distant collimators prior to hitting the close–in collimators.

With standard beam tracking programs checking optical approximations the minimum internal diameter for close–in collimators positioned at various distances from the IR was determined consistent with condition (c). The minimum beam pipe diameter consistent with conditions (a) and (b) was then calculated. Finally the thickness of shielding in the vicinity of the collimators was found. The distance of the close–in collimators was adjusted to minimize the ID of the beam pipe while maintaining low radiation levels in the tracking chambers.

Finally, the addition of a 500μm cylindrical titanium liner[6] to the beryllium beam pipe was deemed advisable to absorb the secondary fluorescent X–rays (to which Be is essentially transparent) generated by hard synchotron X–rays striking the collimators.

Fig. 1 shows the final optimized configuration. The close–in tantalum collimators are at 1 meter from the IR, to absorb mostly hard electrons and photons. Surrounding them is a layer of heavimet which shields against secondaries produced in the process. The Ti liner placement is also shown.

With this configuration the main residual source of background arose from synchotron X–rays in the energy range of 10-100 KeV generated in the low–beta quadrupoles by the beam halo and Compton back scattered from faces of the collimators. The beam halo was fed both by Coulomb scattering in the residual gas of the machine vacuum and by beam–beam interactions and was much larger than would be estimated from the Gaussian beam spread associated with quantum fluctuations in the emission of synchotron radiation.

The observed backgrounds levels are approximately that which would result from the conversion of two 50 KeV photons per beam crossing in the Vertex Chamber gas. Under the final operating conditions this approximated a dosage rate for the anode wires of the tracking chamber of 10^{-9} C/cm/sec. This background was relatively insensitive to beam conditions and steering and even with a small diameter beam pipe, the MAC detector was less sensitive to beam steering than the other PEP detectors.

3. Chamber and Shielding Mounting

The beam pipe, shielding and VC were mounted as a unit to provide the required strength. A "strong-back" structure was used to support the beam-pipe, shielding, tantalum scrapers and the outer pressure wall of the VC enclosure. Once assembled, almost no space was available for access to the chamber. Controls, gas flow and pre–amps were therefore located remotely from the chamber.

To replace existing detector elements in the shadow of the new shielding, part of the latter was made in the form of active detectors constructed of bismuth germanate (BGO) crystals to provide continuous calorimetry coverage to within 4.5° of the beam line. These are also shown in fig. 1. Readout of these scintillators was by light sensitive diodes which could operate in the magnetic field. Their successful operation is the first application of this technology in a collider experiment.

The gas volume was connected at both ends to feed pipes, permitting either flow-through of gas or operation by filling and sealing off the chamber for extended time periods with remotely operated solenoid valves. The former mode kept the gas at constant density. The latter mode was used to maintain gas purity against contamination.

Each tube had its own coaxial cable providing high voltage to the wire and transmitting the ionization signals. Bundles of cables were vacuum cast in epoxy blocks. The epoxy filled the cable shielding interstices and provided a sealing surface for a gas tight penetration of the pressure vessel end walls.

The final system was rugged and trouble free and no disassembly was required to maintain operations.

4. Design and Construction of the Vertex Chamber

4.1 DESIGN

The Vertex Chamber was formed from "straws" stretched between aluminum end-plates separated by a 0.6 mm Be spool piece closely fitting the Be beam pipe. The first layer had a total of 40 straws, with no more than 25μm clearance between them. The second layer also had 40 straws, fitted in a close-packed configuration with the first, so that the dead space between straws in one layer was covered by a wire in the other. This pattern insured that if two tracks occurred on one side of a straw, so that only that closest one to the wire was recorded in layer 1, the second was that recorded in layer 2 (it being closest to

the wire there.) The other layers were configured in similar fashion, the third and fourth layers each having 54 straws and the fifth and sixth each having 68. The spool arrangement made assemby of straws and wires very easy.

A drawing of the end-plate is given in fig. 2, and a photograph of the chamber during construction is shown in fig. 3.

4.2 CONSTRUCTION

The straws were obtained commercially, with the assistance of the HRS group. They consisted of two layers of 50μm aluminized mylar, cut in strips, and wound spirally on a mandrel of diameter 6.9 mm. The surface resistivity of the aluminum coating was 0.8Ω per square. The layers were held together with contact cement. The tubes delivered by the manufacturer maintained remarkably uniform tolerances, inner diameters being the same to within 10μm and were straight to within 100μm. They were selected for cleanliness and lack of blemishes, and cut to 432 mm lengths.

These tubes were then mounted on the spool by use of 3.45 mm holes in the endplates. A detail of the mounting of straw and wire is shown in fig. 4. The procedure was to glue an aluminum collar with conductive silver epoxy to the inside of the straw, capturing a Delrin plug, which was threaded and slotted for gas flow through the endplate. Electrical ground contacts to the straws were made directly from the collar to the endplate on one end, and made via a spring between collar and the other endplate. The plugs were held by nuts on the threaded parts of the plugs extending through the plates, and these were adjusted for about 500 g force on the straw. The plug was drilled for the insertion of a metallic feed-through, with a 100μm hole to accommodate the wire, and this was seated in the plug as shown in fig. 4.

The 30μm gold plated tungsten wire was drawn through the mounted straws by use of a self supporting wire, threaded into the feed-throughs, and one feed-through was crimped over the wire. The other end of the wire was strung on a pulley and had a 100 g weight attached, so that when that end was crimped it had the proper tension. The tension was checked by placing a magnet near the straw and driving an oscillating current through the wire. This caused the wire to resonate at a frequency proportional to tension. If this tension was out of tolerance the wire was restrung.

The completed chamber, with its cabling, was then slipped over the beryllium beam pipe which was then welded to the reducing sections (see fig. macfig), and a 2.54 mm thick aluminum cylinder was passed over the assembly to form the outer wall of the pressurized volume.

4.3 ELECTRONICS

Each tube of the VC was directly coupled via coaxial cables to electronics outside of the detector. Since the characteristic impedance of the tubes was $\sim 330\Omega$, the other end of the tube was terminated with a 330 ohm resistor AC grounded by a 6 kV 100 pf capacitor. The coax served as both a signal and positive high voltage connection. RG179B was chosen for its small diameter (2.8 mm), good high voltage capability, high characteristic impedance (75Ω), and heat resistance.

Each cable was decoupled from high voltage with a capacitor, and its signal amplified by a LABEN 5242 preamplifier. This ten-pin hybrid included a charge loop fast integrator followed by a pole zero cancellation network and a line driver, and had a 30 Mhz response with very low input noise ($\sim$ 2000 electrons.) Provision was made for input test pulses, fed to individual amplifiers through 1 pf capacitors.

The output of each channel was connected in differential mode through $\sim$ 5 m of "twist and flat" cable to two discriminators, with separately adjustable thresholds. The dual scheme was chosen so that the lower level discriminator output, suitably delayed, could be gated by the higher level discriminator. Thus low amplitude pulses not from real tracks were rejected without sacrificing the timing precision obtainable using a few-electron level discriminator. The circuit utilized the Plessey SP9687 dual comparator chip which exhibites very fast transition times ($\sim$ 1ns) with little slewing and is capability of operating reliably at 1.5 mV thresholds.

The discriminator outputs provided stop signals for standard time to voltage converters (TVCs), and the latter were read by the existing MAC scanning modules. These are described in another article[7]. The standard crossing signal, derived from the PEP rf signal, provided the start pulse for this system.

5. Gas Pressure and High Voltage Control

In order to insure that the time to distance relationship remained stable, the gas flow system was designed as follows. Gas from pressurized cylinders of the mixture was fed through Polyflo tubing to one side of the chamber, and a similar return line from the other side was exhausted to the atmosphere by a vacuum pump. The flow was controlled by manually operated regulator valves and by remotely operated valves at the chamber.

Gas pressure and temperature were monitored by sensors in the VC and on the input and output gas lines. These sensors suffered a DC shift in their output voltage when the MAC solenoidal field was on, but were otherwise stable. The sensors were obtained from Analog Devices Corp.

The flow was set for $\sim$ 1 gas change per hour by setting needle valves, and obtaining fine regulation with a small diaphragm valve. The latter was sensitive to temperature gradients and had to be thermally isolated from ambient drifts. Long term wander was easily controlled by human intervention a few time a week. A further dedicated automatic system used the temperature and pressure sensors to monitor gas density. If the density went outside a window of $\pm 0.75\%$, the solenoidal valves at the chamber would be closed on the appropriate side until the density returned to within tolerance. This system operated very occasionally, and was essentially a safety feature.

No mechanism for regulating temperature was used. This was because the temperature of the chamber was determined by the MAC solenoidal field coil, and this was kept constant by its own cooling system.

The VC gas system kept the gas density to within an rms variation of 0.8% over one week. For the gas used in the VC this contributed to position uncertainty by an amount proportional to drift distance. For the maximum drift distance of 3.5 mm the effect was about 14μm.

High voltage was supplied by externally controlled power supplies. The external controls included interlocks with pressure monitors and current sensors, plus circuits for dual slope ramping of the high voltage.

The chamber was operated at a nominal voltage of 3900 volts, which was just below the transition from saturated-proportional mode to the limited streamer regime. Under normal conditions the current drawn from the chamber was $\sim$ 20μA.

6. Prototype Tests and Results

We now describe the prototype tests which were made during design, and give results which are applicable to the usage of chambers like that described above. The prototype had 16 straws in a 4 by 4 array. The straws were mounted between two end-plates on an aluminum beam with the precision mounting techniques already described. The wire spacing interval was 7.2 mm and the inside straw radius was 3.45 mm. The central wires were 20 μm gold plated tungsten. The prototype was mounted inside a plexiglas tube with endplates capable of withstanding high pressure, and the 16 high voltage coaxial leads from the wires penetrated the endplates through an epoxy plug.

The prototype was run in a SLAC test beam with an 8 GeV/c unseparated negative particle beam produced from a beryllium target bombarded by electrons from the SLAC linear accelerator. The beam contained roughly equal numbers of pions and electrons. The prototype was placed immediately after the final collimator, where beam divergence was only a few milliradians, and beam size was about 3 mm. A small scintillator was placed in the beam ahead of the pressure vessel to provide the zero time signal. The test setup is show in fig. 5.

The electrical circuitry used for the prototype is shown in fig. 6. The tungsten wires were at positive voltage, while the cathodes, consisting of the aluminum layers on the mylar straws, were grounded. One end of each straw was terminated through a 100 pf capacitor by a 300Ω resistor and the other was connected to a total of $\sim$ 5 m of 75Ω coaxial high voltage cable. This cable was decoupled from the high voltage supply by a 1000 pf capacitor, and ended in a preamplifier and cable driver. The sigal was split into two paths, one to a LeCroy 623B discriminator and a LeCroy 2228A Time to Digital Converter (TDC), the other to a LeCroy 2249W Analog to Digital Converter (ADC.)

The scintillation counter signal was used as the common start pulse for the TDC's, for the gating of the ADC's and to interrupt an LSI 11/23 computer which read the CAMAC output of the TDC and ADC modules. Data was accumulated with the "Atropos" system programs[8] developed at SLAC.

An additional test setup used a small "staggered straw" arrangement consisting of a single layer of straws with three spaced as before but with the fourth straw offset vertically by one straw radius. This device was inserted into a small test box that could be evacuated or pressurized. This additional test setup was easy to modify and was used to check the effects of different wire radii on resolution and performance.

6.1 INVESTIGATION OF PROPORTIONAL AND LIMITED STREAMER MODES

As noted in the introduction, an optimal strategy for obtaining best drift time resolution over small drift distances is to use the arrival time of the first electron[3] of the ionization swarm. This requires high gas gain and/or high quality preamps to ensure that single electron signals exceed the electronic noise. In the prototype tests we investigated performance both at relatively low gains in the proportional mode, at moderate gains in the saturated proportional mode and at high gains in the limited streamer[9], or LS mode. Tests were made with an absolute pressure of between one and four torr.

The gases used for the tests were argon-ethane in a 50:50 mixture, argon-isobutane in 75:25 mixture, and argon-carbon dioxide in 75:25 mixture. We were able to observe LS pulse production in all the above gases except for the last. Most stable operation at high gain, *i.e.* best plateau and pulse uniformity, was obtained for the highest pressures.

We used an Fe^{55} source, with its 5.9 KeV X-ray emission from the manganese K_α transition, to provide a calibration signal. This radiation penetrated the thin straw wall and released $\sim$ 240 electrons in a single cluster. Additionally we used pulses from single electrons produced by photo-emission from the cathode surface to provide single electron calibrations. Light from a source such as a flashlight penetrated the thin aluminized mylar and ejected, via the photo-electric effect, a strong flux of individual electrons from the aluminum cathode. The actual photo-sensitivity of the cathode surface depended strongly on the previous history of the cathode surface. The single electron signal was also used on-line to calibrate discriminator levels directly in terms of number of electrons required to trigger the TDC discriminators.

As a function of voltage, the pulses observed from a test straw showed transitions from the proportional mode to saturated proportional mode to LS mode at critical voltages which were dependent on gas and pressure. Remarkably enough, with highly quenched gases that would normally be classified as being in the saturated proportional mode at 1 torr, with slow increases in Fe^{55} gain as a function of voltage, we observed that at higher pressure the single electron induced pulses showed the discontinuous jump in gain characteristic of limited streamer operation. Beyond this transition the single electron induced pulses became nearly identical to those induced by the Fe^{55} source. The pulses also had the characteristic very fast rise ($\sim$ 3 ns) and fall times associated with streamer formation.

Illustrative of this combined mode are typical results shown in fig. 7. It shows the mean pulse height observed in these tests as a function of straw voltage.

Note that although the single electron response increased by almost two orders of magnitude at the LS threshold, the Fe^{55} pulses were already saturated and did not change appreciably.

The characteristics of the LS mode at elevated pressure differed in another essential respect from restricted streamers observed at lower pressures by other authors[9]. Pulses associated with a Sr^{90} beta-ray source, which produces non-localized ionization, did not give predominantly single streamers, but rather gave large and variable pulses which could have up to ten times the amplitude and pulse duration of those produced by Fe^{55}. This can be explained by the Fe^{55} photon producing a tight cluster of ionization which produces a single streamer and a deadened region with a spatial extent of a few hundred microns. The lightly ionizing track, on the other hand, presumably produces a variable number of separate streamers, each with its own dead region. In spite of this variability, the sense wire supported count–rates in excess of 10^4 Hz/cm in the LS mode without appreciable dead-times.

The voltage-plateau for these single-electron streamers depended on the gas used. The plateau ended with the occurrence of characteristic regenerative breakdown pulses, separated in time by the electron drift time from anode to cathode. These clearly arose from UV photons, produced in the initial avalanche, causing photo-emission of electrons from the cathode. The cathode photo-sensitivity decreased and the gain plateau increased significantly with charge collected. (We could not distinguish whether this change was caused by surface clean-up or surface contamination). Typically, after "running-in" a straw, plateaus for single electron streamers were of the order of 800 V for heavily quenched gases at 4 torr.

Smaller wire diameters ($20 - 40\mu$m) showed the combined property of long plateaus for both saturated proportional gain for large pulses and saturated streamer behavior for single electrons. These wire diameters therefore provide an option of running in either mode. For this reason we chose to use 30μm wires for use in the final chamber.

The use of LS pulses in drift time measurements has advantages aside from the obvious one of high gain ($\sim 10^7 - 10^8$.) These pulses are quite uniform, and have initial rise times shorter than a few nanoseconds, corresponding to electron collection rather than ion drift. In the saturated proportional mode, pulses from minimum ionizing particles have 50-100 times the amplitude of pulses from single electrons. Therefore in the LS mode the first electron produces almost the entire pulse height, as opposed to a small fraction, so that in the proportional region cross-talk must be less than $\sim 1\%$ to trigger reliably on the first electron, while in LS mode thresholds can be raised, and cross-talk becomes unimportant.

6.2 CROSS-TALK

In the following subsections, we present studies of position resolution which potentially can be realized in practice if the problem of cross-talk between channels can be handled. The magnitude of the problem of course depends upon the particular electronic circuitry used.

In our test setup we measured cross-talk matrices for the entire system and its parts, using Fe^{55} photons. Elements in the system matrix ranged from 0.3% to 1.5%. The cross-talk was traced to incomplete shielding by the aluminum layer in the straw and to common grounding at the preamp output, in roughly equal parts. Some cross-talk pulses were inverted with respect to the primary pulse, while some were not. The pulses were highly differentiated and frequency dependent; slower rising pulses gave less cross-talk. Timing from cross-talk pulses is significantly slewed with respect to the primary pulses, because the cross-talk pulses are so small. Inverted cross-talk pulses were particularly delayed. We conclude that an upper limit on cross-talk of 0.5% is feasible.

6.3 RESOLUTION AND DRIFT VELOCITIES FOR VARIOUS GAS MIXES

Argon-Ethane, 50:50

Extensive measurements were made with the standard argon-ethane 50:50 gas mixture. Tests were made at 1, 2, 3 and 4 torr absolute pressure, with voltages spanning if possible the LS threshold, and at various discriminator settings. This gas has a drift velocity which is very nearly constant at the electric fields used.

It is instructive to present the results in the graphic form of scatter plots of arrival times on one straw versus another straw. Fig. 8 displays such a plot for the staggered straw array showing the electron arrival time for straw 4, the offset straw, versus the arrival time for straw 1. If the drift velocity were exactly constant then the sum of the two times divided by the drift velocity would equal the offset between the two wires. The scatter plot shows a correlation very close to that expected for a constant drift velocity. Analysis of the small departures from linearity and use of the known straw offset permitted an accurate determination of the drift velocity as a function of position within the straw. The resolution as a function of position was also be determined.

Fig. 9 displays results from the 16 straw prototype with the sense wire plane tilted at an angle of 29° to the beam. This figure shows arrival times for straw 1 versus straw 4 for operation at 4 torr. A cut was made to minimize backgrounds by demanding a very loose track fit of the hits in the other straws. Three regimes are apparent. Tracks crossing the array above or below both wire centers give

rise to the parallel arms of linear correlation with the position within the straws. Tracks passing between the two wires give hits with a connecting negative correlation; the sum of the two time displacements is approximately constant for a saturated drift velocity. These three regimes are clearly seen in fig. 9. Additionally the behavior of tracks passing close to either of the wires can be seen from crossing times close to zero. A track going through the center of a sense wire can form its first cluster at a finite distance from the wire and so can result in a non-zero arrival time. This results in an observed time jitter of $\sim$1 ns (50μm in distance) in the vicinity of the wire. The observations are in agreement with predictions based on a detector threshold corresponding to the first electron arriving at the sense wire.

Use of the information from three straws permits correction for small effects from non-parallelism of the beam. To obtain resolution figures we used the following procedure. The passage of an 8 GeV/c particle through the drift cells was signalled by the occurrence of a scintillator pulse, which initiated the readout of TDC and ADC information. Tracks were selected by requiring either 4 TDC digitizations, or 3 TDC values in the case of determination of efficiency, which were fit to a straight line. Though the χ^2 cutoff was made very loose, in order not to cut off the tails of the distributions, no significant background remained.

For the data selected in this way, fig. 10 shows the distribution of the quantity

$$R = \sqrt{\frac{2}{3}}[\frac{t_1 + t_3}{2} - t_2]$$

which can be shown to have a standard deviation equal to the single wire resolution. The distribution is well described by a Gaussian curve.

We have generally chosen to interpret the rms of the distribution as the position resolution, although it is generally larger than that obtained by fitting a Gaussian. To convert time to position resolution for argon-ethane, we have used a velocity of 50μm/ns[10]. The data of fig. 10 indicates an rms R of 20μm.

Results of similar analyses at other pressures, voltages and discrimination levels are summarized in fig. 11. The highest voltage at each pressure above 1 torr was in the LS regime, where the resolution became essentially independent of the discriminator level. As voltage is reduced, R increases and becomes sensitive to discriminator setting. At 4 torr, resolution is excellent over a considerable range of voltages. At 1 torr, the resolution does not appear to reach a limiting value in a way similar to that seen at higher pressure, and gets rapidly worse with decreased voltage.

The relative independence of resolution and discriminator level in the LS regime confirms the conclusions of the previous section that the first electron to drift to the wire controls the rising edge of the pulse. However, it should also be noted that at high pressures, resolution would not degraded substantially if one were forced to run in the proportional mode, so long as the voltage remained near the LS threshold.

The dependence of resolution on distance from the wire is shown in fig. 12 at 4 torr for two voltages and two discrimination levels. The best overall result was for 4 kV, in the LS regime, where the effect of diffusion was barely visible. At 3.7 kV, in the proportional regime, resolution was only slightly worse but showed an expected deterioration near the wire, especially at high discriminator levels. The explanation is that electron collection proceeds substantially more slowly than for tracks away from the wire, causing the leading edge of the pulse to be more ragged. These results are compared to a solid and a broken line representing respectively which represent the result of a Monte Carlo simulation of the collection geometry[2]. Agreement is good for a choice of diffusion constant $\sigma_d = 170\mu$m-cm$^{-\frac{1}{2}}/\sqrt{P}$. This value agrees with our direct independent measurement of this quantity.

We have also explored the effect of tracks traversing the straws at an angle to the long axis of the straws. For operation at 4 torr we show resolution as a function of angle in fig. 13a. It is clear that the increase in effective ion density along the projected track path with angle gives improved resolution. Fig. 13b shows the time resolution curve obtained at $\theta = 70°$. It is double peaked because the fourth wire of the array had a 50μm offset with respect to the other three. This resolved the position ambiguity and made it possible to measure such small resolution.

Argon-Isobutane, 75:25

Argon-isobutane mixtures are promising because heavy molecules are good quenchers. We tried a 75:25 mixture in conditions essentially identical to those used for the data of the previous section. The transition from proportional to LS modes occurred at roughly the same voltage as with the argon-ethane mixture. The results for resolution are so close to those of the previous mixture that we do not show them. We conclude that this mixture would be interchangeable with argon-ethane.

Argon-CO_2, 75:25

To obtain good lifetimes of the detector in a high radiation environment it could be imperative to use mixtures without hydrocarbons. A possible choice is argon-CO_2. We tried this in a 75:25 mixture at 2 and 4 torr.

This mixture does not have a saturated velocity characteristic, but does appear to have a high field plateau, although the actual values in the literature are inconsistent. We have used the values of Ma *et al*[11] as given in the compilation of Ref. 10 and when converted for our straw geometry and 3300 volts, we find a velocity dependence on radius which is shown in fig. 14a. In fig. 14b we show our data for this voltage, with time converted to distance according to the velocity profile.

At 2750 volts, resolution had already deteriorated by $\sim$ 50%.

6.4 DRIFT CHAMBER LIFETIMES

The main problem associated with the use of very high gains ($\sim 10^8$ for single electrons and associated average pulse gains of $\sim 10^7$) is chamber degradation. High gain coupled with an intense radiation environment must result in a large average DC current drawn by the chamber and eventual failure due to impurity layers deposited on either the cathode or the anode. We therefore made tests with a variety of gas mixtures. We expected, and have observed, that the use of flat cathodes permits the achievement of relatively long tube lifetimes.

Lifetime tests must be run at substantially higher rates than will be encountered with the actual apparatus, or they will require time greater than that for the ultimate use of the tubes. Such tests almost certainly cause non-linear degradation of tube performance and will result in shorter lifetimes than are likely to be observed under real running conditions. Our tests were made at 4 torr with a 10μCi Fe^{55} source placed next to the straws. The applied high–voltage was sufficient to produce saturated streamer mode pulses at gains corresponding to $\sim$150 mV into 50 ohms. The pulse rate was $\sim$30,000 Hz corresponding to 1-2 μA per cm of wire.

The test straw was contained in a sealed pressurized vessel. The geometry and conditions differed in significant respects from previous tests,[9,12] including the use of pressure, very high gains and a sealed gas volume.

Gases containing a large proportion of hydrocarbons such as ethane or isobutane went into continuous discharge mode after integrated currents of 0.05 C/cm. This discharge was caused by degradation of the anodes by the formation of "whiskers". If a new anode wire was inserted in the straw it would run for a similar period indicating that the problem was not connected with the cathode.

We therefore decided against quenching with organic gases and used CO_2 instead. The best overall gas mixture found was argon:CO_2:CH_4 in proportions of 50:49:1. It could be operated in the LS regime, and had a lifetime of $\sim$1.0

C/cm. Argon:CO_2 50:50 gave a shorter lifetime of ~0.5 C/cm. The former mixture was used in the final chamber.

The use of xenon as an additive[13] was also tried. We have observed clean single-electron streamer mode operation with a plateau of 900 volts and an ability to sustain currents in excess of of 6μA/cm in an argon:xenon:CO_2 30:20:50 mixture at 4 torr pressure, without any added hydrocarbon quencher. In addition to the enhancement of avalanche multiplication by a large factor through the Penning effect Xenon appears to quench UV feedback, probably via its hard UV absorption bands centered at 1400 and 1200 AU.[14] Despite the absence of hydrocarbons we observed anode degradation in this gas mixture after 0.5 C/cm. This degradation was associated with a disappearance of the voltage plateau for streamer operation with this gas mixture, but the tube would still operate with normal resolution, in proportional mode, using the standard 90:10 argon-methane gas mixture.

6.5 Conclusions from prototype tests

The results of resolution studies using the argon-ethane gas mixture showed good agreement with Monte Carlo predictions[2] when values for the longitudinal diffusion constant of about 170μm-cm$^{-\frac{1}{2}}$-torr$^{\frac{1}{2}}$ are used. The resolutions obtained under a wide variety of conditions for gases pressurized to 4 torr in a tube or straw configuration lie in the range 10-40μm. At this level experimental precision is likely to be limited not by track resolution but by multiple scattering and other such constraints[15].

Straws can be operated at very high gains and can be used in a mode giving single electron saturated streamers combined with strongly saturated Fe^{55} pulses. This mode showed other qualitative differences from the restricted streamers observed at lower gas pressures. The streamers appear be confined to a region with spatial extent of only a few hundred microns and counting rates in excess of 10^4 Hz/cm do not cause appreciable deadtimes.

Lifetimes for straw operation are good and similar to those observed for flat-cathode detectors used in other applications. The gas we have found to be best for lifetime is a mixture of argon:CO_2:CH_4 in ratio 50:49:1 which gave a lifetime corresponding to an integrated charge on the anode of ~1 C/cm. This mixture is reasonably well quenched, permitting operation at high gain with good chamber lifetime.

7. Experience with the Actual Chamber

The MAC vertex chamber was completed and installed in October 1984. The background currents from circulating beams did not rule out operation in the LS mode. However the decision was taken to run at voltages just below the LS threshold, so as not to risk termination of the experiment by premature ageing.

Since installation the actual chamber has not requred access. Four wires have broken or drawn high current and were disconnected during the experiment. No noticeable degradation of output pulses, or of position resolution has occurred in the remaining wires.

We describe below the procedures used to obtain the ultimate 50μm resolution of the chamber.

7.1 ELECTRONICS CALIBRATION

After installation of the entire system, non-trivial problems had to be faced regarding environmental electronic noise and pick-up. The source of the pick-up was finally traced to the switching of the TVC gates which were located close to the discriminator crates just outside the PEP shielding wall. Reduction of this noise to below the level of the white noise of the amplifiers was achieved for almost all tubes by relocating the TVC crates. Ten tubes had poor ground connections at the chamber and had higher noise; these had to run at higher thresholds than the others. The final configuration allowed the remainder to run at a threshold equivalent to two primary electrons.

In order to provide a good starting point for calibration of the TVC system a channel by channel parameter determination was performed. With a drift velocity of 100μm/ns close to the wire (dropping to 8μm/ns at the tube wall,) TVC contributions to timing uncertainty had to be less than 0.5 ns in order not to affect the chamber resolution significantly. The following calibration scheme achieved this. Pulses were injected at each preamplifier input by a CAMAC controlled delay generator and a response curve mapped for every channel. Calibration data were collected over a time range about 30% greater than that of the real data. For each TVC channel the functional relation between the delay and the digitized time was fitted to a quadratic polynomial. It was required that the product of the linear and quadratic coefficient be negative, as expected from the expansion of a negative exponential. The fitted parameters of the TVC were quite stable; it was necessary to perform the calibration procedure at only two or three month intervals.

The overall preformance of the TVC system, considering that it was not originally designed for VC precision, was very satisfactory; the slopes of the 324 channels were found to deviate by less than 1%. This implies measured times within 1 nsec for the same number of counts at half maximum drift distance. Here the contribution of the quadratic term was of the order of 0.5% (roughly 0.5ns). The time offset of each channel was determined with the same procedure.

The final t_0 values for each tube were obtained, along with wire position corrections, from actual particle tracks. This procedure is explained below.

7.2 OFF–LINE CALIBRATIONS AND TRACK IDENTIFICATION

Time-to-distance calibration

The time-to-distance relationship for the gas mixture used was determined as part of an iterative procedure in which the drift velocity parameters plus the individual wire positions as a function of axial length were found. Two track events from Bhabha scattering events were selected according to criteria based on the response of other components of MAC. These tracks were then matched to corresponding hits in the VC and an overall fit made which included the wire survey and time conversion parameters. The ensemble of such track fits was used to obtain optimized values of these parameters.

The time-to-distance relationship was approximately $r \sim \sqrt{t}$, reflecting the linear dependence of velocity with electric field in this gas mixture and the r^{-1} field dependence. This can be seen in fig. 15 where the drift time observed in a given tube is compared to the distance interpolated from other hits on the same track. However the final function was determined by fitting the smoothed experimental data in 1 ns intervals by means of a cubic spline procedure.

Geometric survey of VC positioning

The orientation of the VC relative to the CD depends on four offset parameters. These are the x and y values at z=0, where z is along the beam axis, and the tilt parameters $d\phi/dz$ and dr/dz. These parameters were determined by comparing, at the interface between the VC and CD, the mismatch of track segments independently measured by the CD and VC. The matrix required for a χ^2 minimization was accumulated from these miss distances and the inversion of this matrix provided the four geometric offsets. The offsets were stable throughout the running periods.

Individual wire position and timing corrections

Obtaining the best resolution required software calibration of the TVC zero time offsets, ramp slopes, and wire offsets in both slope and position for each

wire individually. To do this, survey tracks from Bhabha scattering events were selected as described above but were constrained in a fit to come from a common vertex, to have opposite charge, to have momenta close to the beam energy and to have a good χ^2 when the uncertainties of the measurements were taken from the previous iteration. The same fit was then made with each of the VC hits dropped in turn, and the differences between measured and predicted hit positions were saved. The accumulated differences were then required to be zero in the average by altering the velocity and survey parameters in a correlated fit.

The computer program, in a single pass through the survey tracks, made the above described fits for all wires and produced a survey constants file. The program also determined the overall resolution without correction and that to be expected after correction. Such a procedure applied to six layers can improve random systematic errors by a factor of $\sqrt{1/6}$. The dominant corrections were associated with chamber endplate rotation and tilt. The overall position resolution was improved from 80μm to 50μm with this procedure. A second iteration of the procedure did not improve the resolution.

Pattern Recognition

Track segments were first obtained by separate pattern recognition programs for the VC and CD. The CD vectors were found by the procedures used prior to the construction of the VC. The VC algorithm is of some special interest, as it exploits the geometry of the tube placement. A brief description of this program follows.

VC track vectors were identified by first searching the double layers for associated pairs of hits. With the overlapping geometry of the VC double layers, at radii R_1 and R_2, a radial track produces hits in these layers with impact parameters r_1 and r_2 related to the tube radius r_0 by

$$\frac{R_2 r_1 + R_1 r_2}{R_2} \approx r_0$$

Such associated pairs are with high probability associated with a track and the sign ambiguity (*i.e.* which side of the wire was struck) is also resolved. These associated pairs were then used as starting points for the search for hits on tracks traversing the VC.

After CD and VC tracks had been found separately, vectors in the VC and CD systems were then matched to form single tracks. About 70% of tracks present were found by this procedure. The hits used for these tracks were then removed from further consideration. The search for the remaining tracks was continued

by extrapolation of the unmatched CD tracks into the VC and collecting and fitting the unused hits in the VC which lay within a track road. This procedure was especially effective for very low momentum tracks and tracks from long–lived decay vertices.

The final step in the procedure was to fit the combined track taking into account multiple scattering, to search for and include additional hits that lay within 4σ of the fitted track and to drop hits from the fit that were outside a 6σ tolerance.

A subset of events were scanned, using graphical representation, after the above described procedures were implemented and the various cuts were optimized. No obviously bad misidentifications or identifications that could have been improved by human interventions were observed.

7.3 Observed Resolutions

After the above procedures were used to determine the survey constants, drift velocity profile and electronic response parameters, the track fit residuals could be used to obtain the single wire position resolution. This was done by assigning to each hit a weight equal to the inverse square of the resolution for the measured drift distance and by requiring that the resulting χ^2 distribution be correct for the appropriate number of degrees of freedom in the fit. The resolution function found in this way is shown in fig. 16.

The loss of resolution for small distances is largely explained by the greatly increased drift velocity, and by the increased sensitivity to ionization fluctuations. The latter effect arises because at large distances there is little difference in minimum drift distance from the closest clusters (a Jacobian peak in fact occurs,) while at the wire the mean drift distance is one half the average cluster separation. It should be noted that this loss of precision near the wire will occur in *any* drift chamber, but for large cells these regions are a relatively small fraction of the sensitive area and on average become unimportant. In the case of the straw chamber, the averaging is done over layers, so that the majority of hits on a track have excellent resolution.

The ultimate test of the system is of course the accuracy with which tracks are extrapolated to the event vertex. A measure of this is shown in fig. 17, where the mismatch between tracks of Bhabha scattering events when extrapolated to the VC center is shown. The width of this distribution is then $\sqrt{2}$ times the vertex impact parameter resolution, which is measured to be 90μm.

Finally, we show in fig. 18 the VC hits observed and the tracks fitted to them, for an event interpreted as coming from τ-lepton pair production, with each τ

decaying into three charged particles. The hits are represented by circles, to which the track associated with them should be tangent. It should be noted that the figure is quite representative of the low number of accidental hits observed.

Although the resolution figures given above are a good representation of the ultimate straw chamber preformance, it should be pointed out that they apply to low multiplicity events. In the typical multihadron event, with 10-20 tracks, the resolution deteriorated by about 50%. Possible sources of this effect are electronic saturation effects, cross-talk, and increased acceptance of incorrect hits. We cannot account completely for this loss of resolution.

8. Overall Conclusions

We have described the design and construction of a vertex chamber using a coaxial tube geometry, colloquially known as a straw chamber. We have justified the choice of this technique, in a way intended to help other experimenters decide the most appropriate choice for them. Briefly we chose it for its ruggedness (loss of one cell not interfering with the operation of the others,) its ease and speed of construction, its optimal geometry for timing on the first arriving electron, its small cell size and hence low occupancy allowing use of single hit electronics, and its potential for long life in an environment with high radiation levels. These characteristics are not specific to our experiment, but are required by others, such as those projected for future high luminosity hadron colliders.

We have discussed the procedure we used to estimate shielding needed to place a chamber at about 3 cm from the PEP beam line. The resulting configuration resulted in extremely quiet operation of the VC.

We have also given the results of tests with a chamber prototype used in a test beam to study the behavior of tube output pulses as a function of electric field, pressure, and gas mixture. We have shown that the resolution improves dramatically with pressure both because inter-cluster distance decreases and because diffusion is decreased. Increased pressure also allows more stable operation in the limited streamer mode, where a single electron can generate a pulse which rises as fast as, and is as big as, one from a large ionization cluster. The best resolution is obtained in the LS mode. However in this mode the average currents are much larger than for the proportional mode, and too rapid chamber deterioration can occur.

Lifetime studies of a variety of gases were presented. The best lifetime, along with LS response, was obtained with a gas mixture of argon:CO_2:CH_4 in the ratios 50:49:1. The lifetime was ~ 2 C/cm.

Finally the computer algorithms used to obtain the best resolution, and to find and fit tracks, were described. These were used to estimate the effective position resolution of the device, which was 50μm, and the vertex impact parameter resolution, which was 90μm.

We conclude that the technique of constructing a chamber with straws has completely fulfilled the requirements of our experiment, and that the characteristics of such a chamber permit a wide range of tracking applications in high radiation environments.

9. Acknowledgements

We gratefully acknowledge discussions we have had with E. Iarocci, D. Rust, and J. Jaros. Next, the Precision Paper Tube Co. of Wheeling, Ill., must be thanked for their cooperation in manufacturing the straws. We also wish to thank R. Coombes, E. Askeland, J. Schroeder, J. Escalera, and J. Broeder for their superb technical work. We would especially like to acknowledge and remember the late T. Pulliam, the engineer responsible for the installation. Finally R. Gearhart's help with the test beam setup is appreciated.

REFERENCES

1. D. Rust, SLAC-PUB-3311, April 1984.
2. G. Chadwick and F. Muller, MAC Internal Memo No. 683, Feb. 1984.
3. J. Va'Vra, SLAC-PUB 3131, June 1983.
4. J. A. Jaros, Stanford 1982: Proceedings, Instrumentation for Colliding Beam Physics (1982); SLC Workshop Note No. 51, Dec. 1981
5. A. Boyarsky, SLC Workshop Note No. 2, Feb. 1983.
6. C. T. Hoard, SLAC-TN-82-3, October 1982.
7. E. Fernandez *et al.*, SLAC-PUB 4048 (Aug. 1986), and to be published.
8. C. Logg and P.W. Clancey, SLAC Electronics Dept. ELDDOC No.25, 1983.
9. E. Iarocci, Nucl. Inst. and Meth. **217**, 30 (1983); M. Atac and A. V. Tollestrup, Preprint FN-339, Fermilab (1981); T. A. Mulera and V. Perez-Mendez, Nucl. Inst. Meth. **203**, 609 (1982); T. A. Mulera *et al.*, IEEE Trans. Nucl. Sci., **NS-30**, 355 (1983).
10. see, *e.g.*, J. Fehlmann *et al.*, Compilation of Data for Drift Chamber Operation, ETH ZURICH, HPK, TEC DETECTOR GROUP, July 1982. We have also measured this quantity directly.
11. C. M. Ma *et al.*, MIT Technical Report 129 (1982).
12. A. H. Walenta, Proceedings of the 1977 Isabelle Summer Workshop, p. 41, (1977); Results of Fischer, Sobottka and Walenta, quoted by H. Okuno *et al.* in Proceedings of the 1978 Isabelle Summer Workshop, p. 139 (1978); H. J. Hilke, Proceedings of the 1981 Isabelle Summer Workshop, p. 1275 (1981).
13. R. Z. Fuzesy *et al*, Nucl. Inst. Meth. **100**, 2567 (1972.).
14. G. Baldini, Phys. Rev. **128**, 1562 (1962).
15. G. Chadwick, MAC Internal Memo No. 688, Feb. 1984.

FIGURE CAPTIONS

1. Cross section of the MAC Vertex Chamber, shielding and beam pipe assembly, showing the Tantalum scrapers, heavy-met absorbers, and Titanium liner.

2. Layout of the vertex chamber end-plate, showing the arrangement of the 6 layers of tubes.

3. Photograph of the vertex chamber under construction.

4. Detail of the mounting method for straw and wire.

5. Photograph of the prototype array of straws used in the tests.

6. Schematic of the electrical circuit used in the prototype tests of the MAC vertex chamber.

7. Mean pulse height as function of voltage in argon-ethane at 4 torr.

8. Drift times for two straws offset with respect to the beam by one radius, plotted one versus the other. For constant velocity, their sum is constant.

9. Drift times for two straws tilted at an angle of 29° to the beam, plotted one versus the other. The region of constant sum for the times is smaller and two regions of constant difference emerge.

10. Distribution of the resolution quantity R, for argon-ethane at 4 torr, V=4.15 kV. The curve is a Gaussian distribution fitted to the data, with $\sigma = 0.4$ns, corresponding to 20μm resolution.

11. Average single wire resolution as a function of voltage scaled by pressure for various pressures and discriminator levels. The curves are to guide the eye only.

12. Dependence of resolution on distance from the wire, for argon-ethane 50:50 mixture at 4 torr. The solid circles are for 4 kV at which pulses are in the LS regime. Open circles and crosses are for 3.7 kV, proportional mode. Here resolution is not markedly worse, but the region near the wire shows deterioration, especially at higher discrimination level. The broken line is the result of a computer simulation study of pulse formation by ionization in straws.

13. a) Single wire resolution of the straws as a function of the angle θ from normal incidence. The increase of effective ion density with angle appears to give considerable improvement. b) Time resolution curve for the 70° data. The curve is a fit to a double Gaussian distribution with one variance, used

in obtaining the resolutions quoted. The separation results from a 50μm offset of the fourth wire.

14. a) Velocity profile of a mixture of argon-CO_2 in 75:25 ratio used in the straw electric field configuration. b) Resolution found as function of track distance from the wire.

15. Scatter plot of the drift times observed in a single tube versus the position predicted by a track fitted to up to 5 other tubes associated with this hit. The characteristic nearly parabolic relationship for argon-CO_2 mixtures in ratio 1:1 is clearly visible.

16. Effective average resolution of a single wire obtained as described in the text, as a function of drift distance. The average over all distances is 50μm.

17. Plot of the miss distance (difference in distance of closest approach of tracks at the VC center) for Bhabha scattering events. The width of this distribution indicates a vertex resolution of 90μm.

18. Hits in the VC from a τ-lepton pair production event in MAC. The hits are represented by circles corresponding to the measured drift distances, and tracks are fitted to be tangent to these circles.

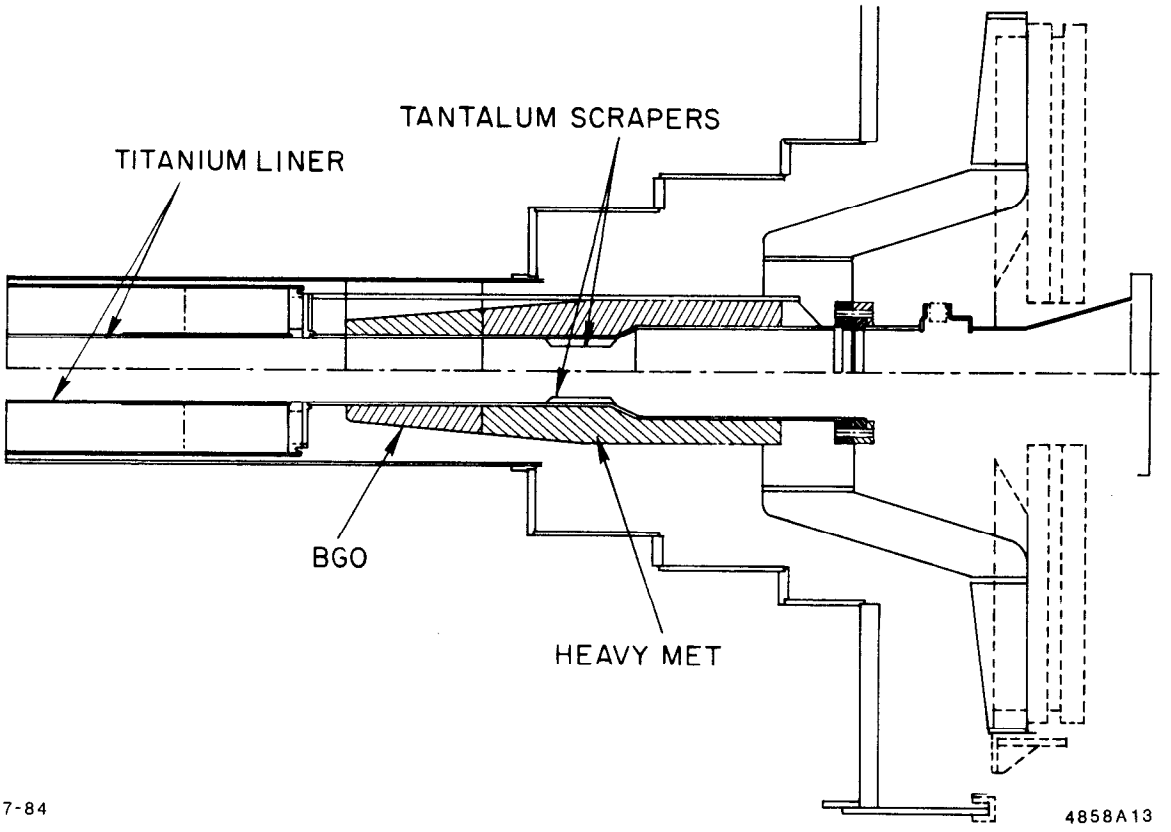
TANTALUM SCRAPERS
TITANIUM LINER
BGO
HEAVY MET
7-84
4858A13

Fig. 1

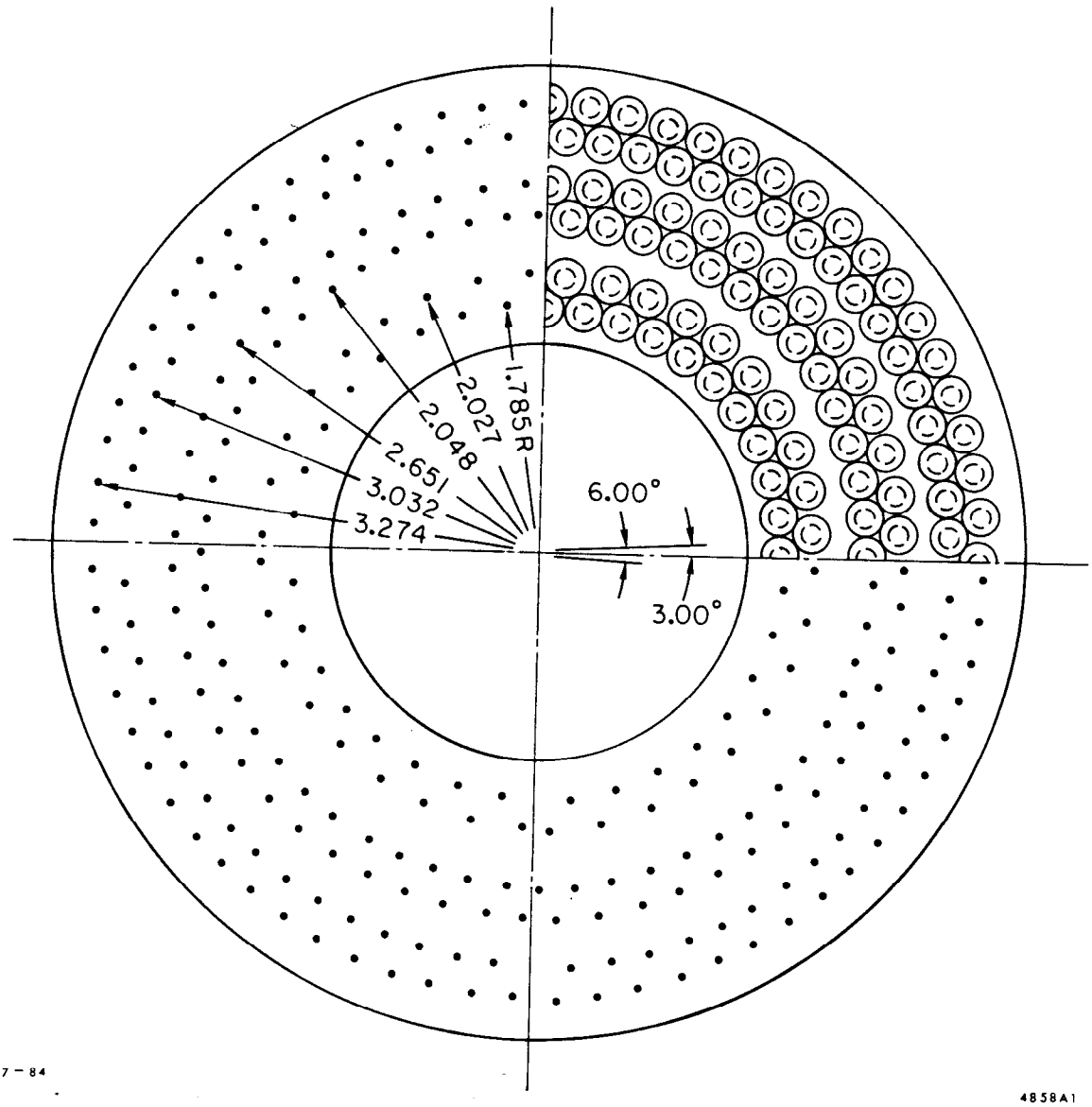

Fig. 2

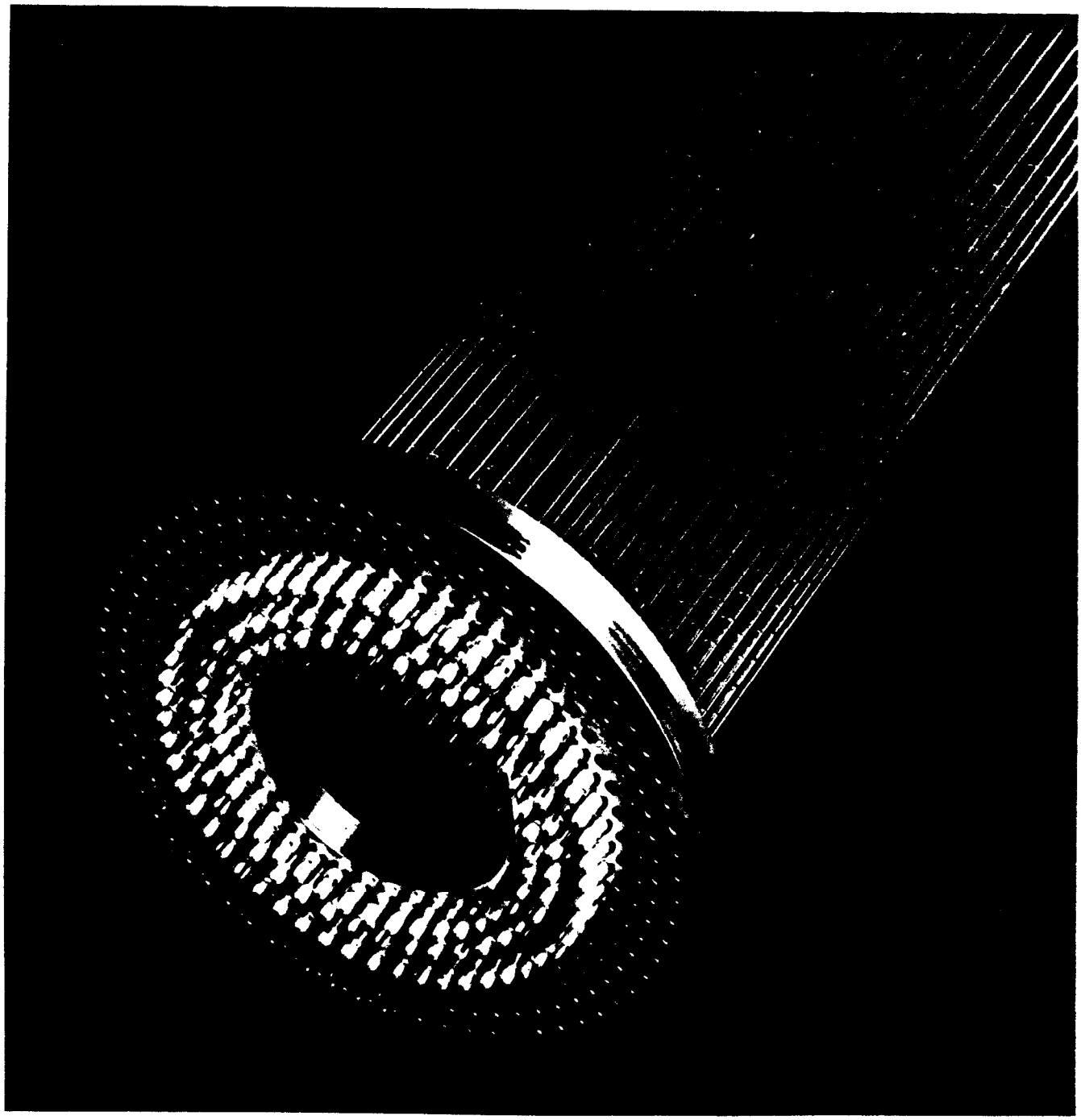

8-84

4858A14

Fig. 3

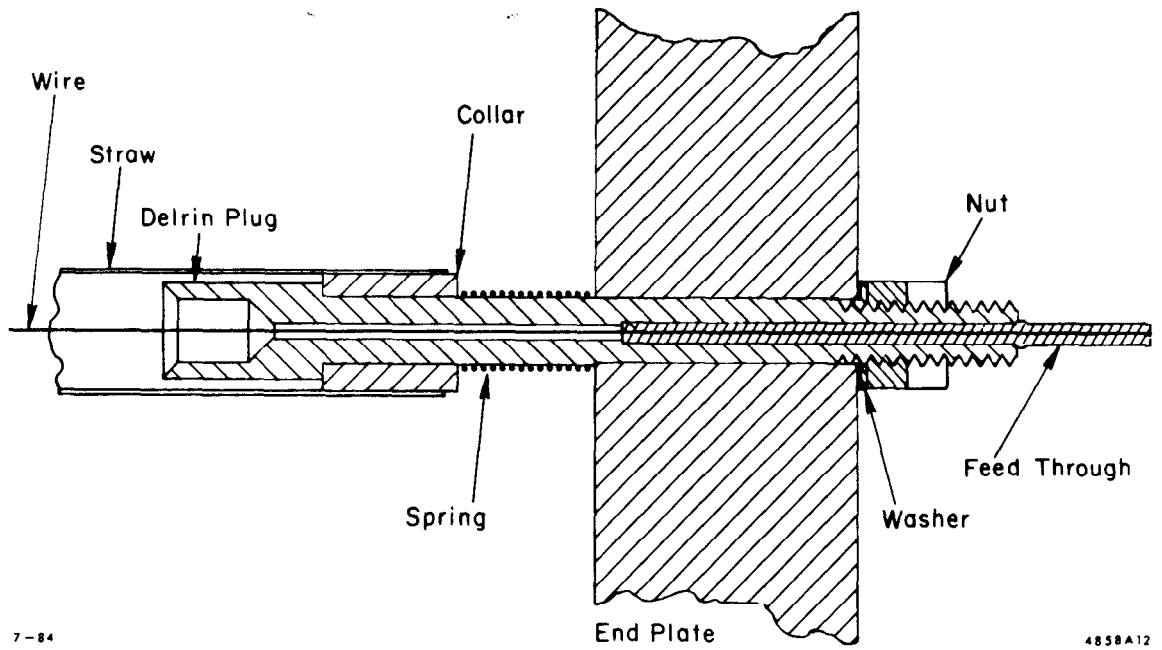
Wire
Straw
Delrin Plug
Collar
Nut
Feed Through
Spring
Washer
End Plate
7-84
4858A12

Fig. 4

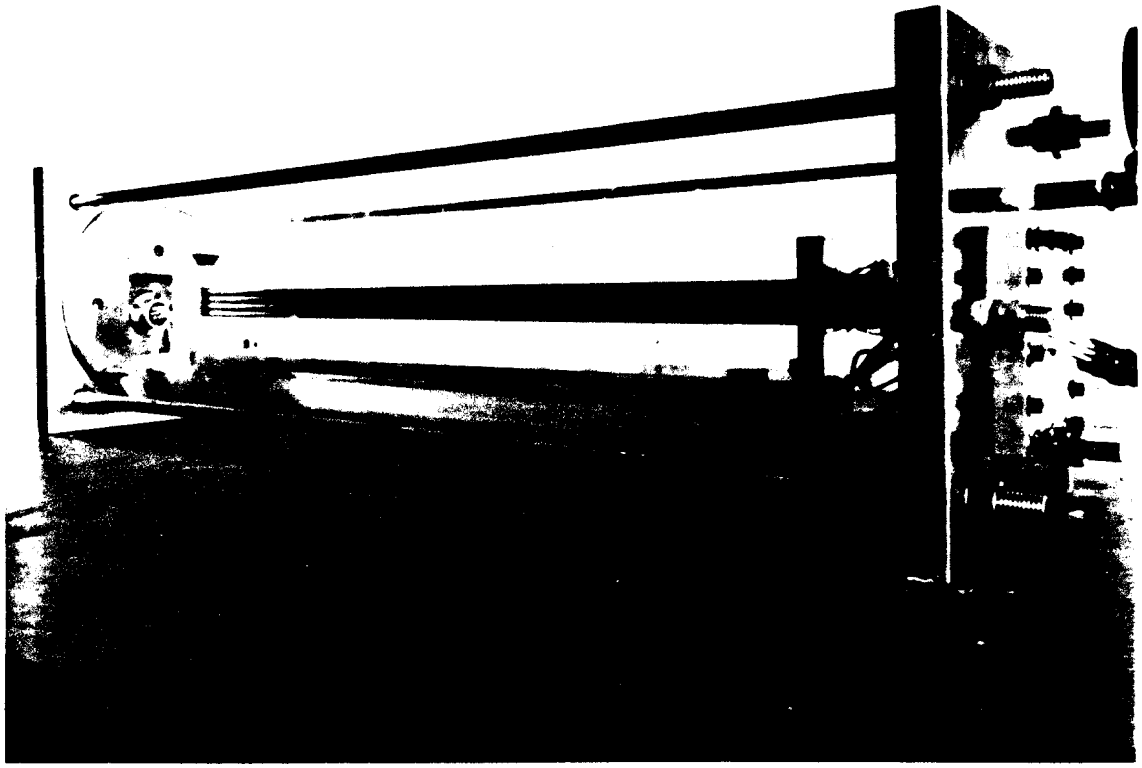

7-86

5476A15

Fig. 5

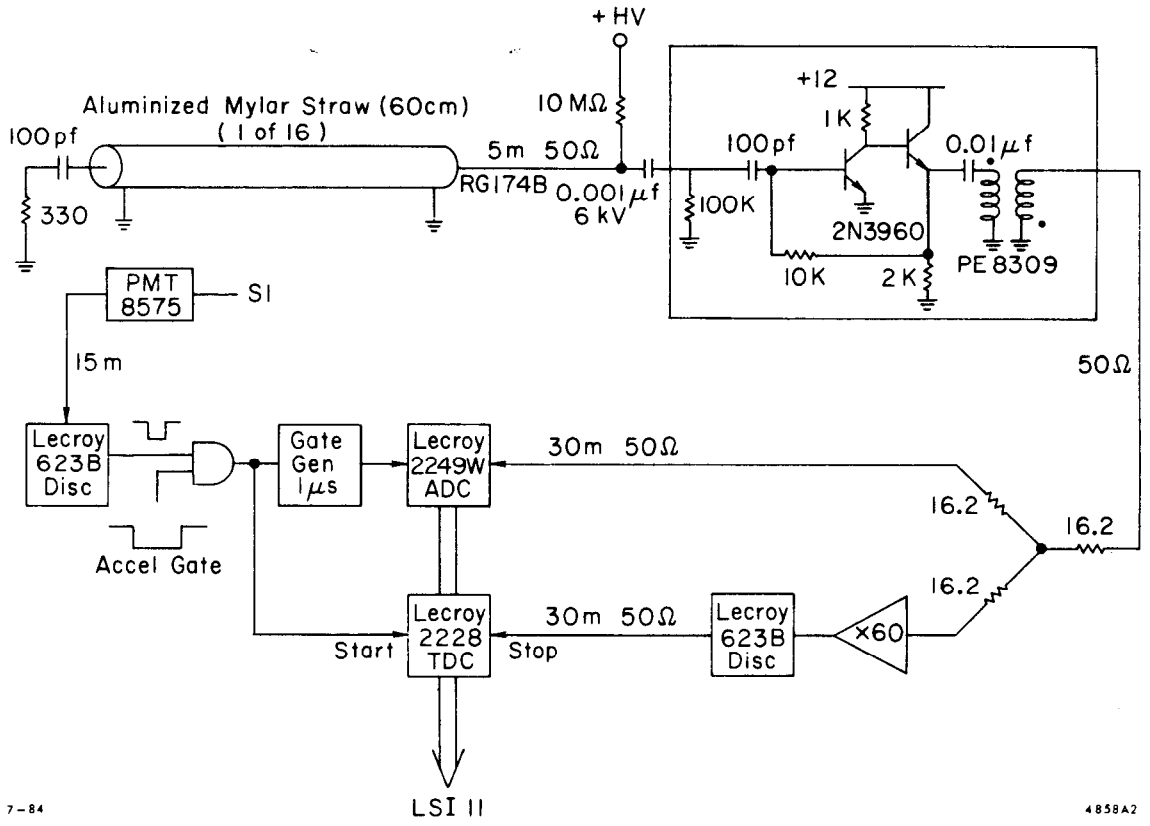
+HV
Aluminized Mylar Straw (60cm)
(1 of 16)
100pf
10 MΩ
5m 50Ω
RG174B
0.001μf
6 kV
330
100K
+12
1K
100pf
0.01μf
2N3960
10K
2K
PE 8309
PMT
8575
SI
15m
50Ω
Lecroy
623B
Disc
Gate
Gen
1μs
Lecroy
2249W
ADC
30m 50Ω
16.2
16.2
16.2
Accel Gate
Lecroy
2228
TDC
30m 50Ω
Lecroy
623B
Disc
×60
Start
Stop
LSI 11
7-84
4858A2

Fig. 6

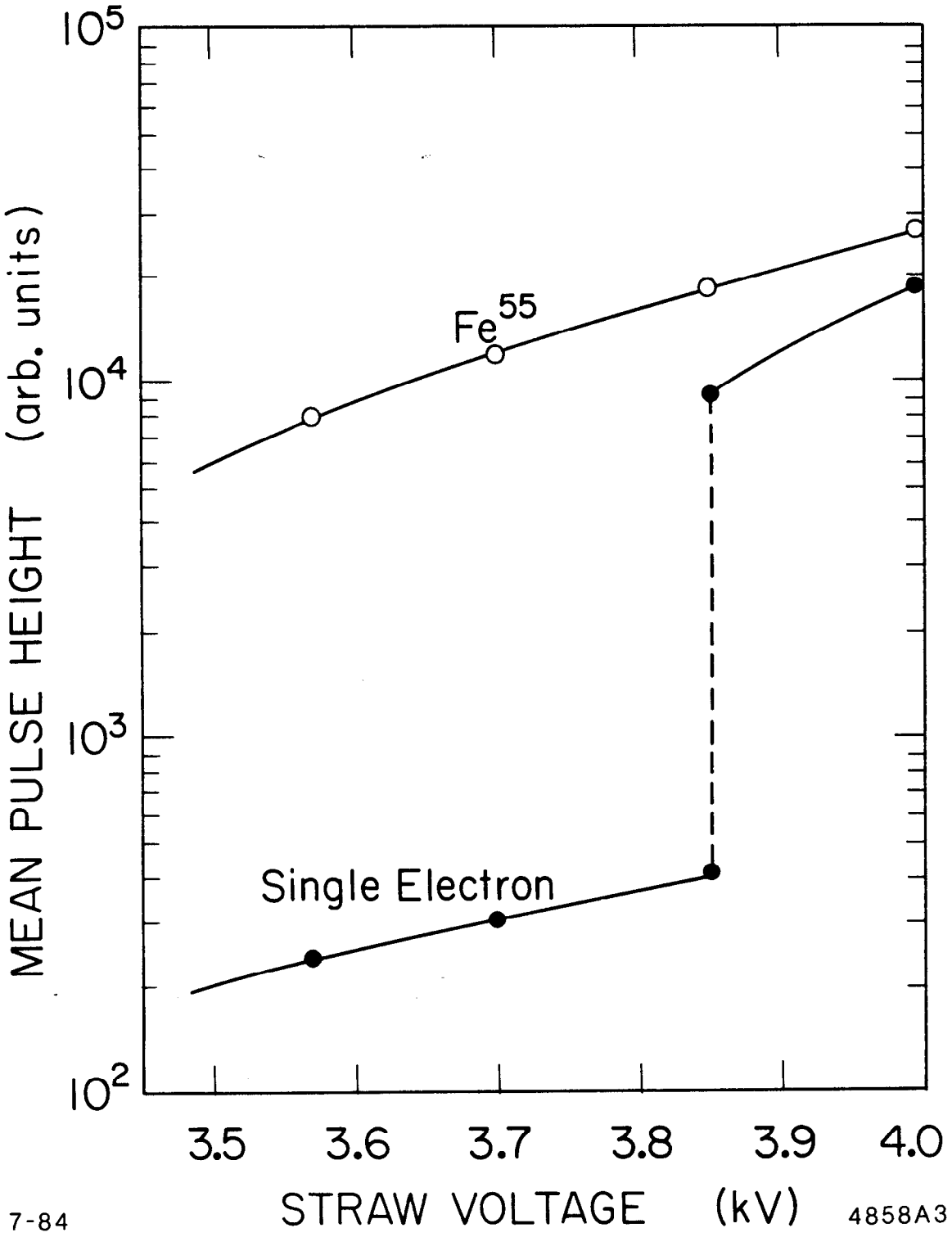
10^5
10^4
10^3
10^2
MEAN PULSE HEIGHT (arb. units)
Fe^{55}
Single Electron
3.5
3.6
3.7
3.8
3.9
4.0
STRAW VOLTAGE (kV)
7-84
4858A3

Fig. 7

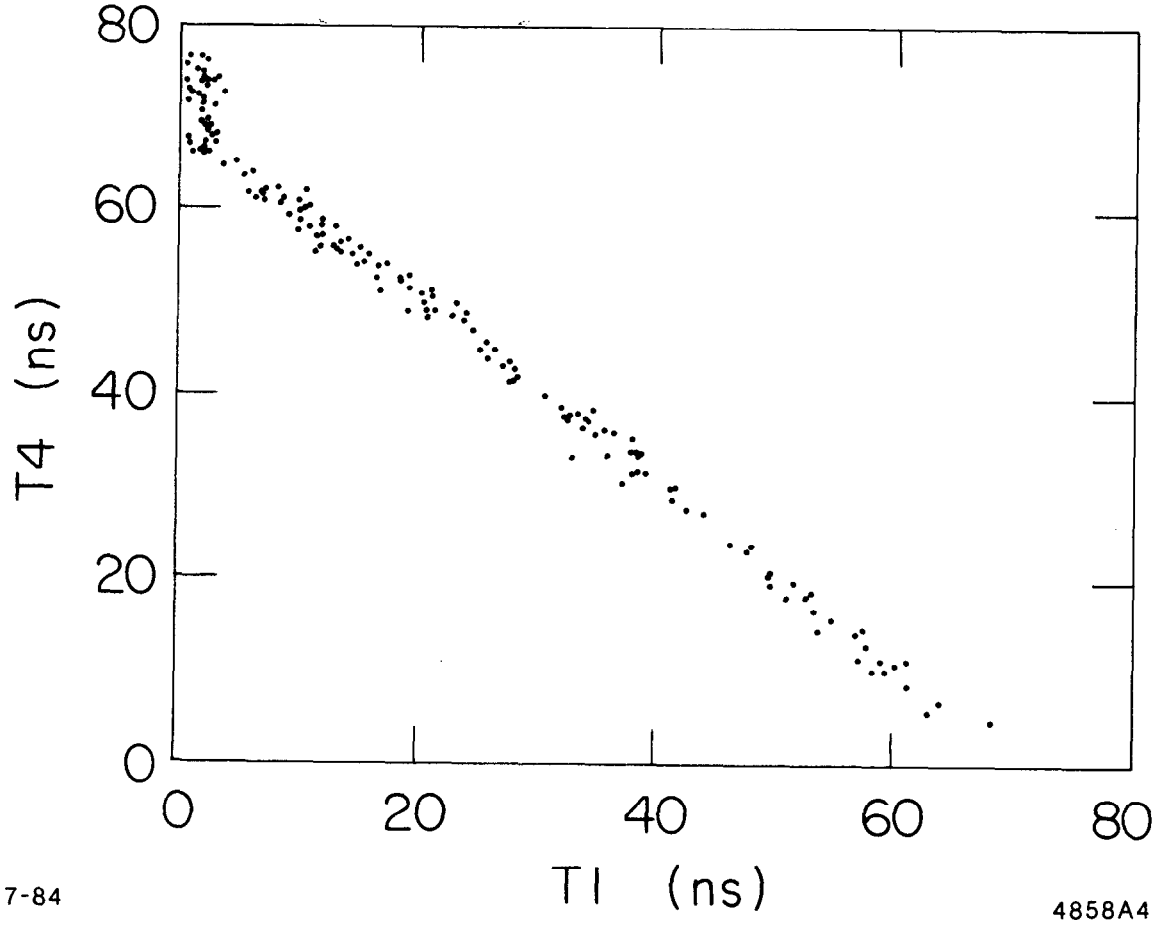

Fig. 8

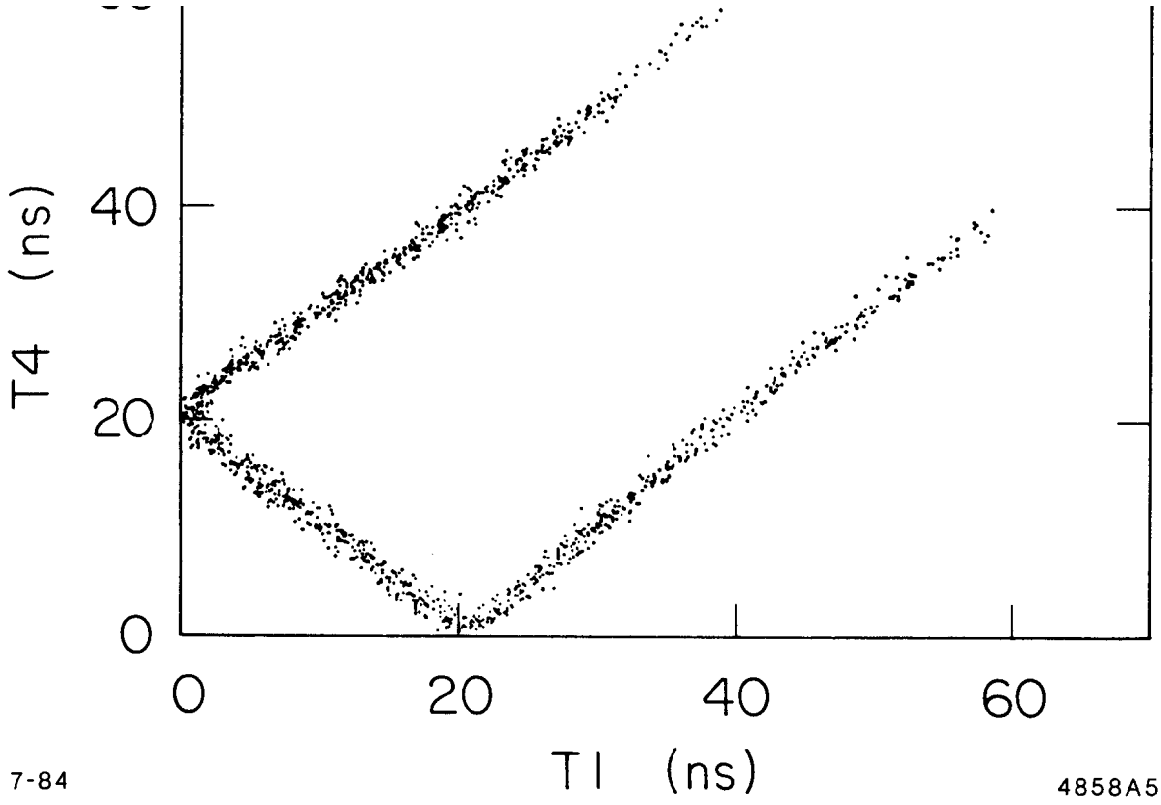

Fig. 9

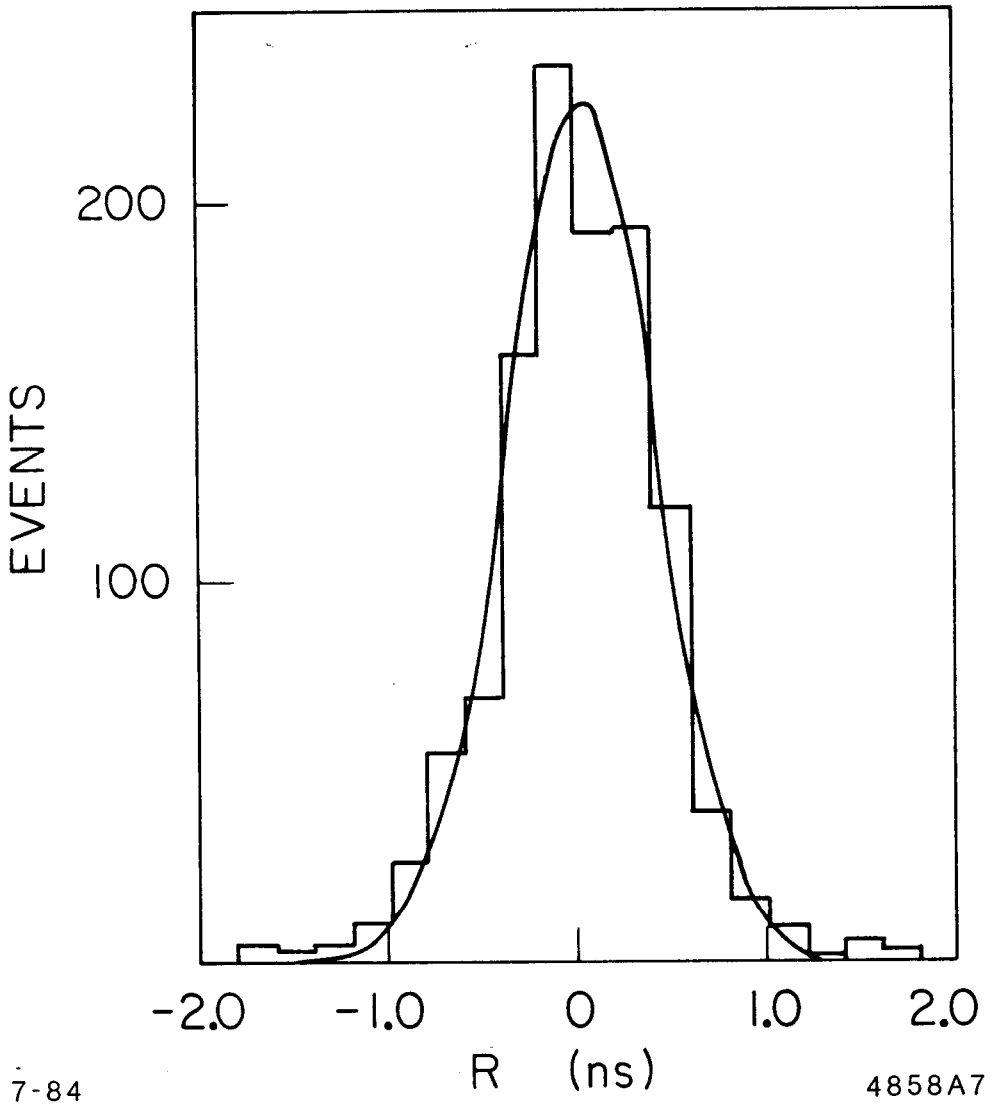

Fig. 10

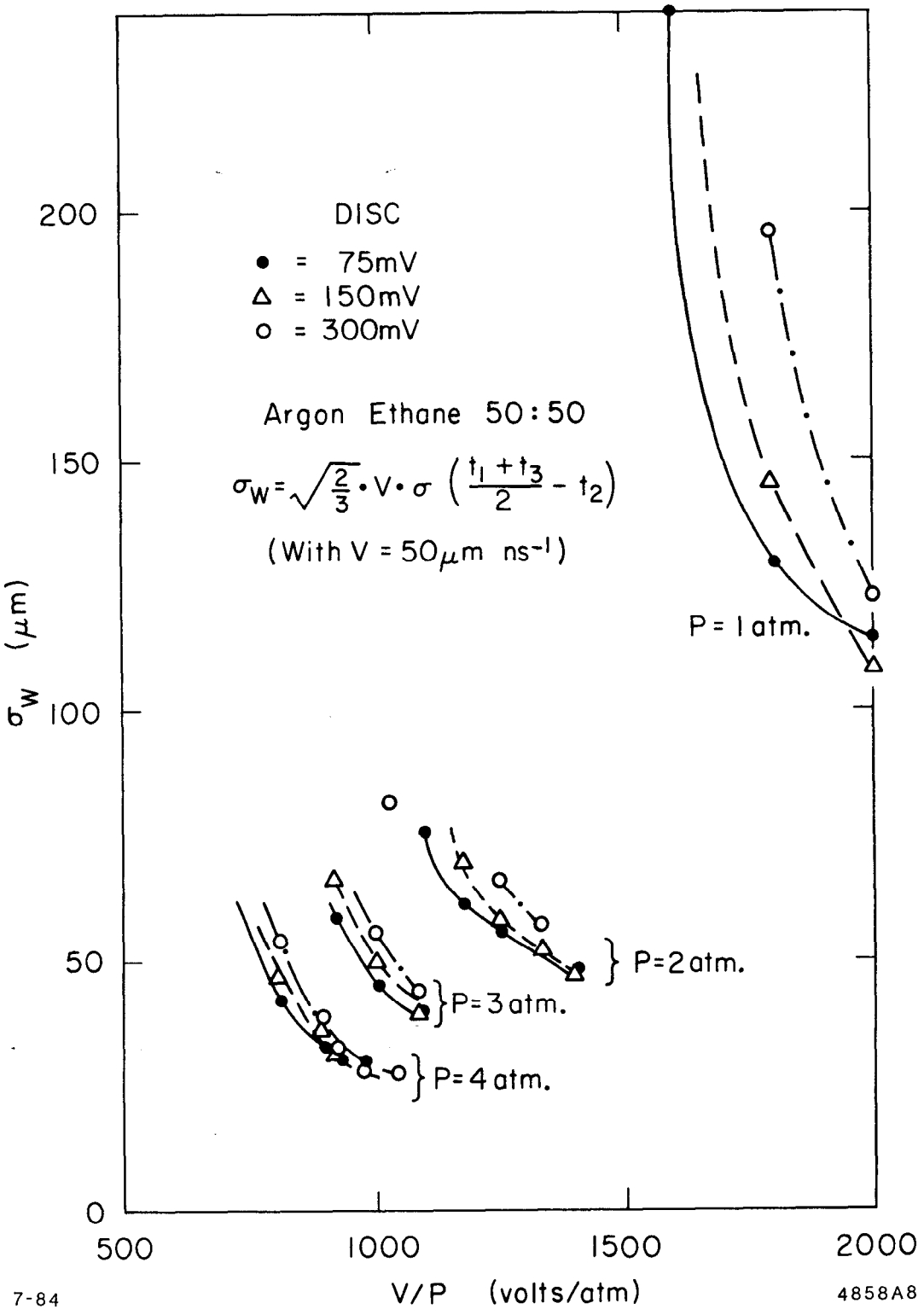
DISC
● = 75mV
△ = 150mV
○ = 300mV
Argon Ethane 50:50
$\sigma_W = \sqrt{\frac{2}{3}} \cdot V \cdot \sigma \left(\frac{t_1 + t_3}{2} - t_2 \right)$
(With V = 50μm ns⁻¹)
P = 1 atm.
P=2 atm.
P=3 atm.
P=4 atm.
σ_W (μm)
200
150
100
50
0
500
1000
1500
2000
V/P (volts/atm)
7-84
4858A8

Fig. 11

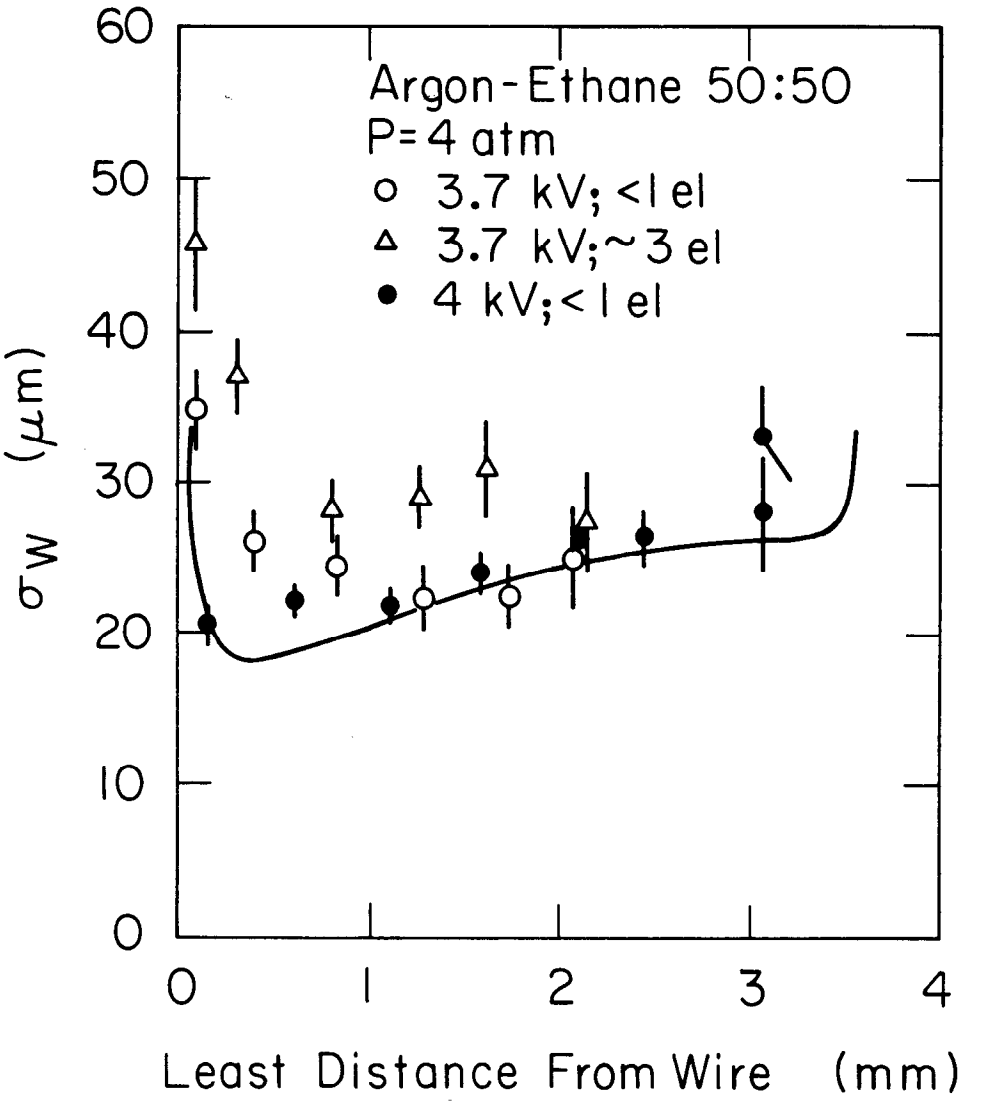
Argon-Ethane 50:50
P=4 atm
o 3.7 kV; <1 el
Δ 3.7 kV; ~3 el
● 4 kV; <1 el
σw (μm)
60
50
40
30
20
10
0
0
1
2
3
4
Least Distance From Wire (mm)
7-84
4858A9

Fig. 12

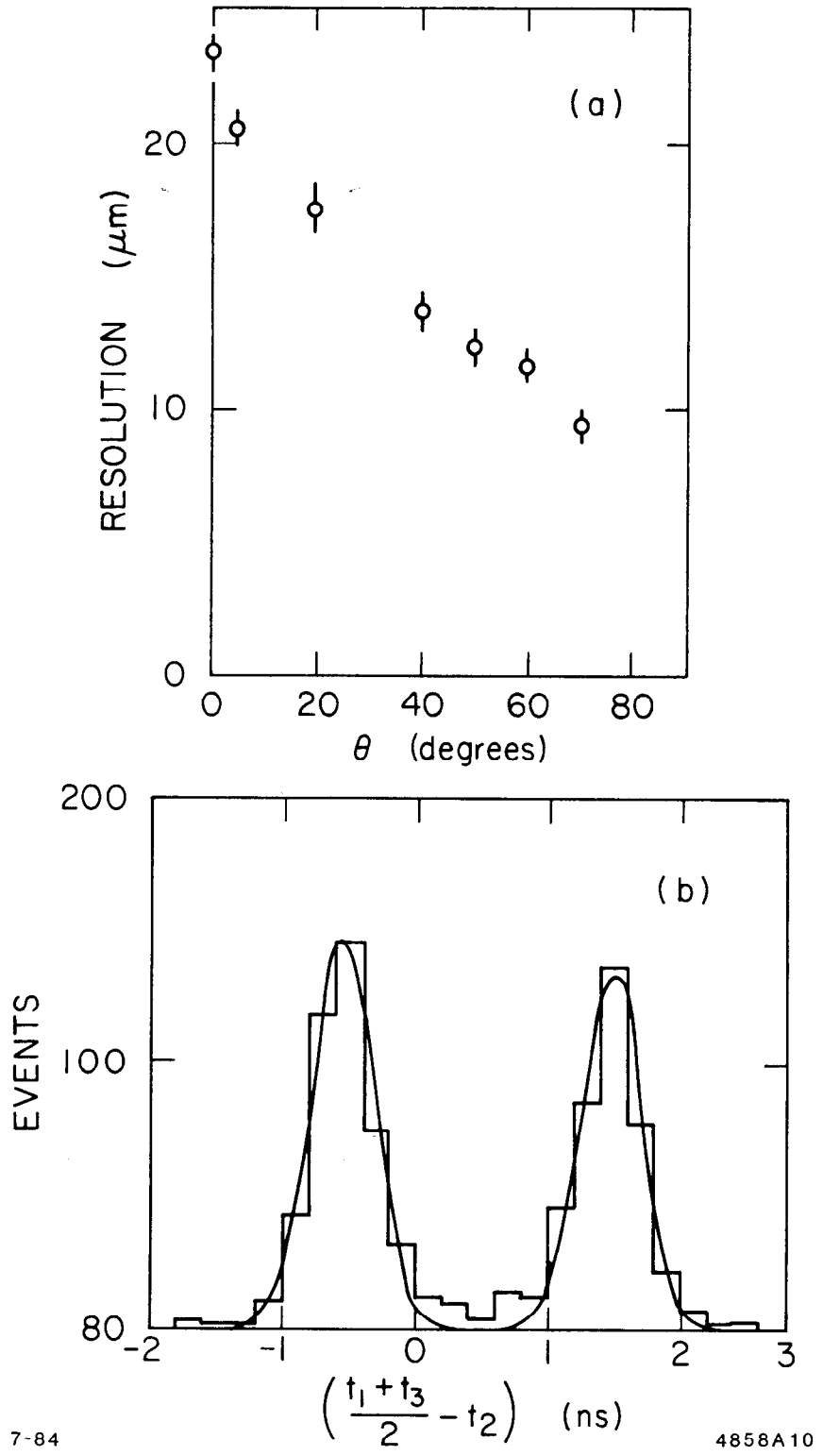
(a)
RESOLUTION (μm)
20
10
0
0
20
40
60
80
θ (degrees)
(b)
EVENTS
200
100
80
-2
-1
0
1
2
3
$\left(\frac{t_1+t_3}{2}-t_2\right)$ (ns)
7-84
4858A10

Fig. 13

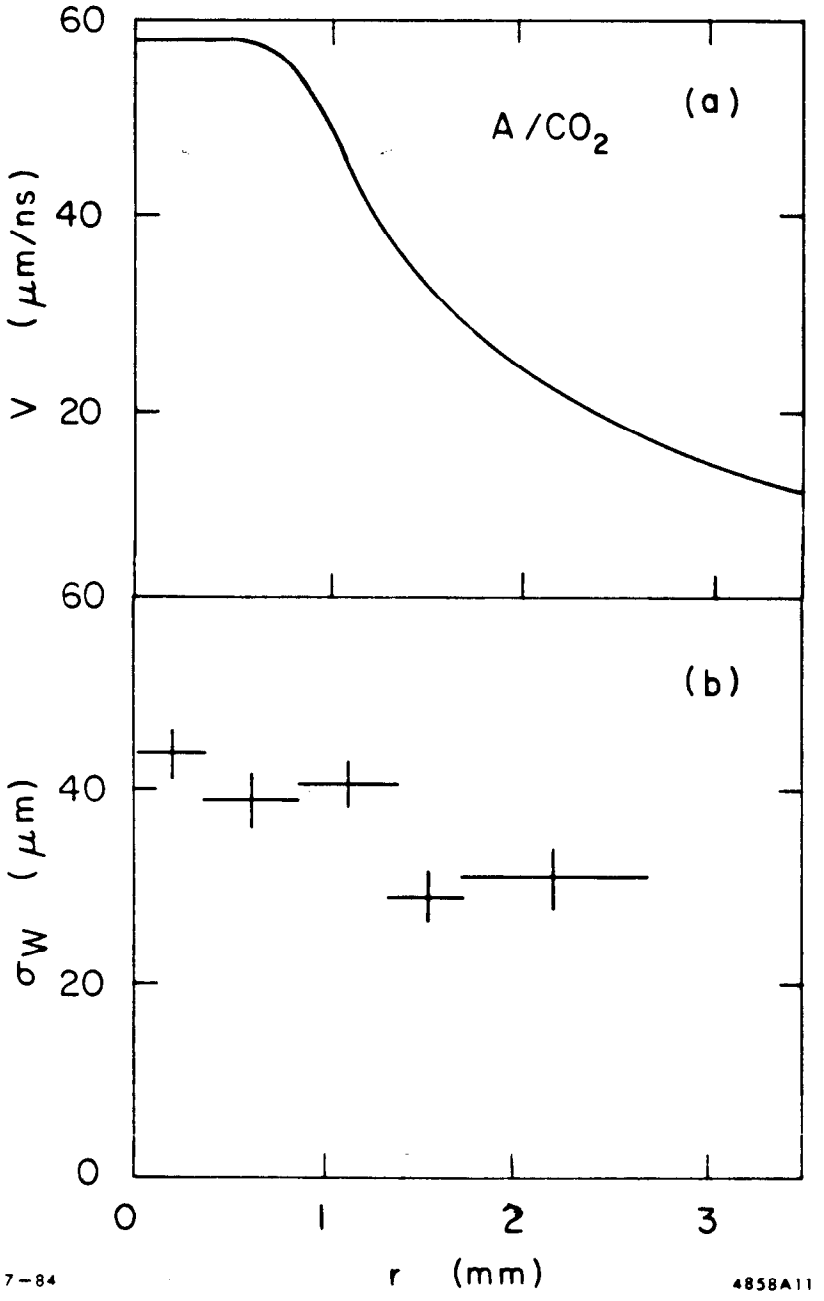

Fig. 14

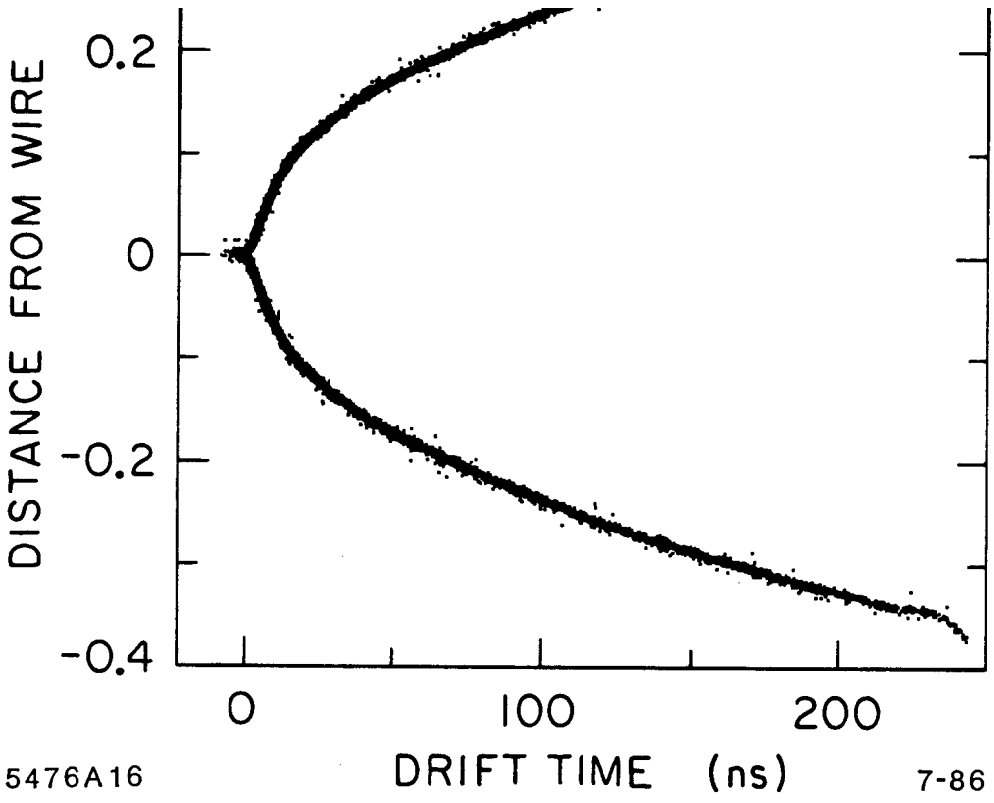
DISTANCE FROM WIRE
0.2
0
-0.2
-0.4
0
100
200
DRIFT TIME (ns)
5476A16
7-86

Fig. 15

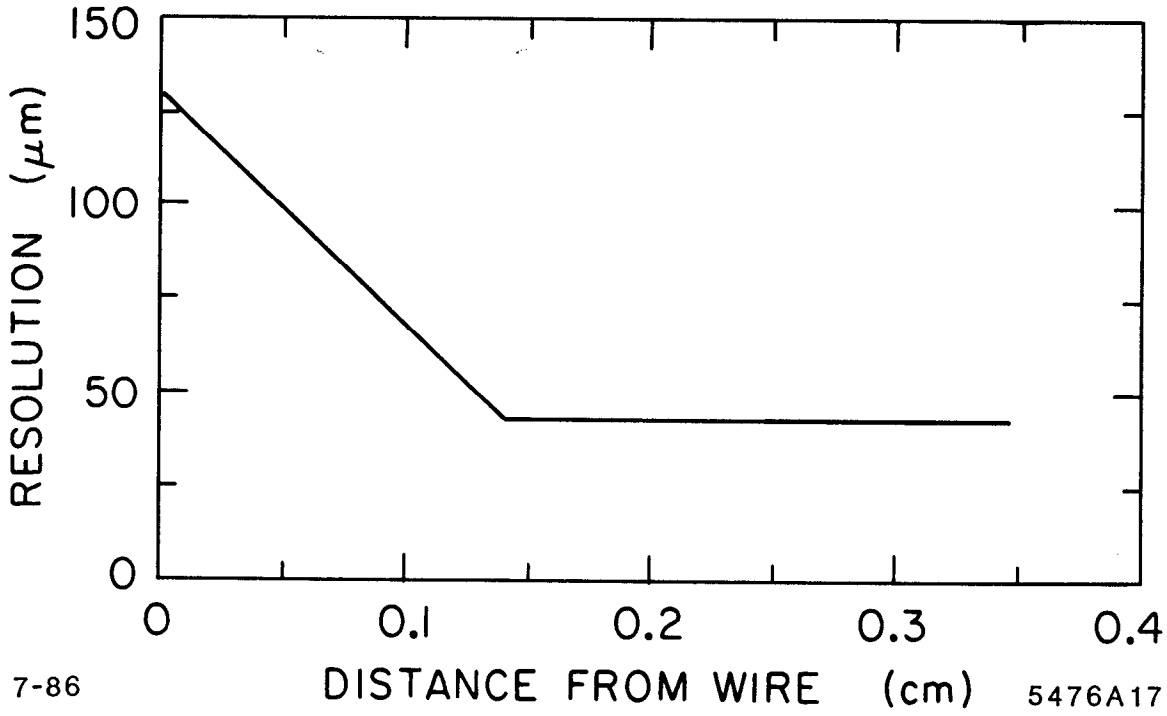
150
100
50
0
RESOLUTION (μm)
0
0.1
0.2
0.3
0.4
DISTANCE FROM WIRE (cm)
7-86
5476A17

Fig. 16

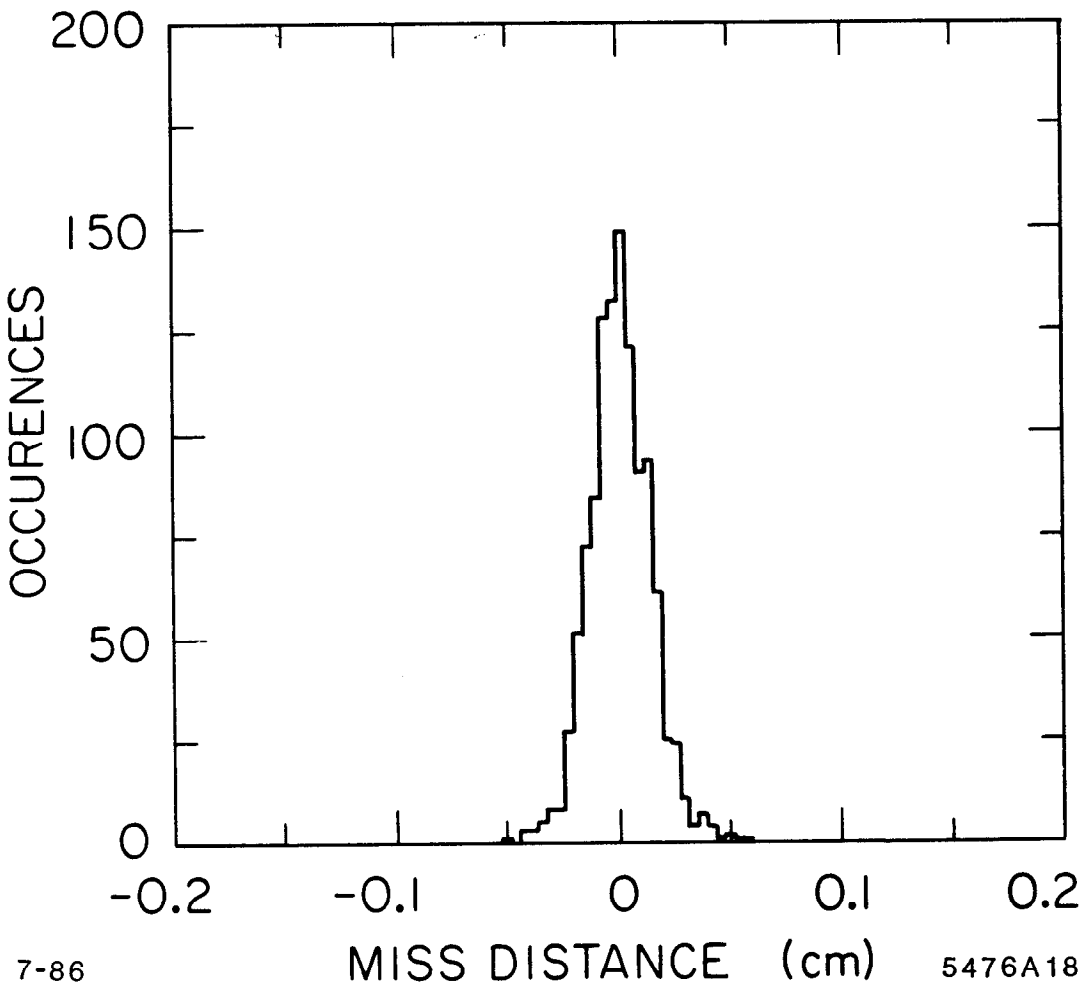
200
150
100
50
0
OCCURENCES
-0.2
-0.1
0
0.1
0.2
MISS DISTANCE (cm)
7-86
5476A18

Fig. 17

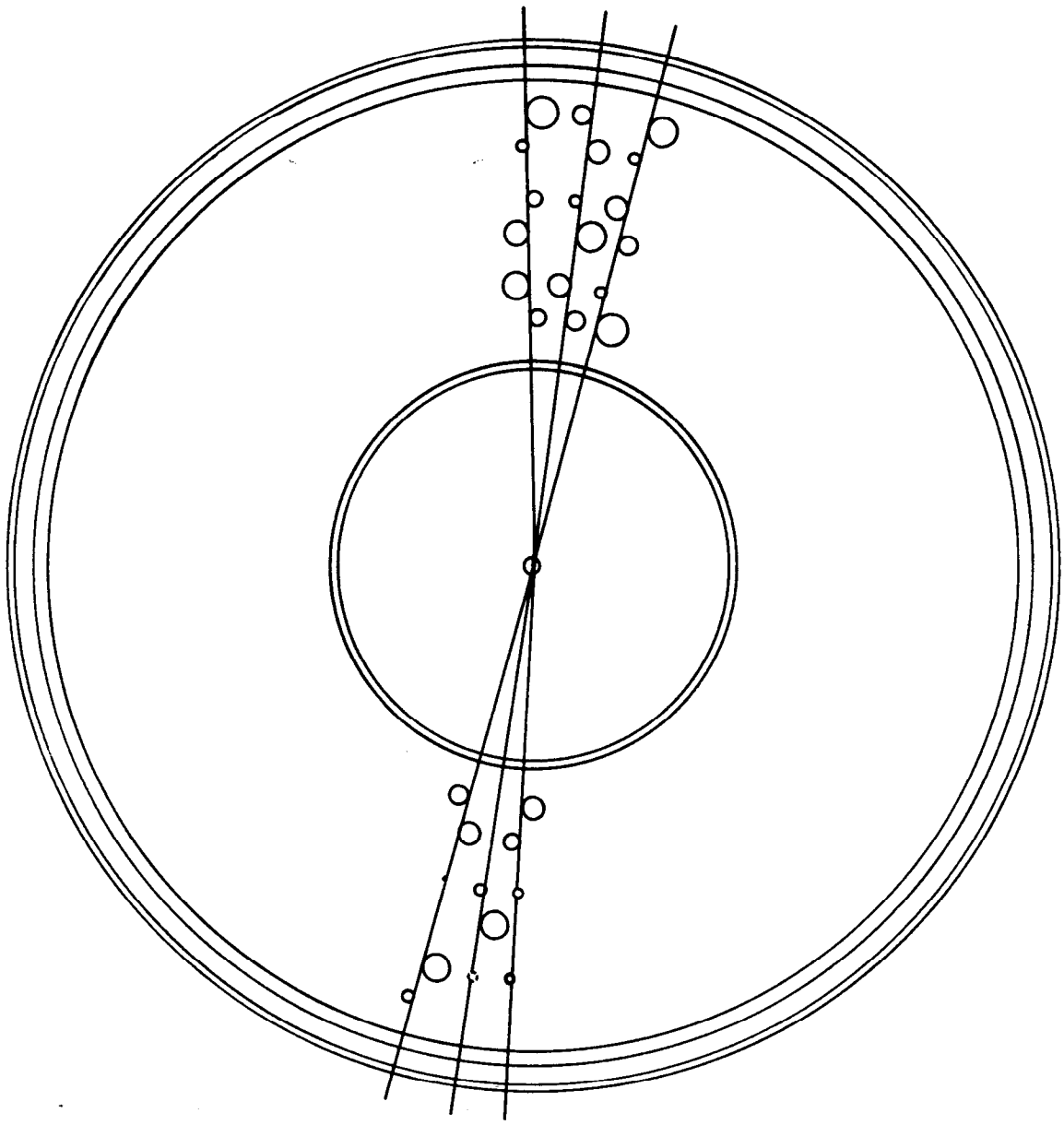

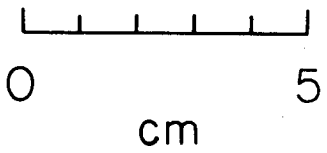

7-86
5476A14

Fig. 18